Title

The HOIL-1L ligase modulates immune signaling and cell death via mono-ubiquitination of LUBAC

Authors

Yasuhiro Fuseya[1,2], Hiroaki Fujita[1], Minsoo Kim[1,3], Fumiaki Ohtake[4,5], Akira Nishide[1,3], Katsuhiro Sasaki[1], Yasushi Saeki[4], Keiji Tanaka[4], Ryosuke Takahashi[2], & Kazuhiro Iwai[1,6*]

Affiliations

[1]Department of Molecular and Cellular Physiology, Graduate School of Medicine, Kyoto University, Sakyo-ku, Kyoto 606-8501, Japan.

[2]Department of Neurology, Graduate School of Medicine, Kyoto University Hospital, Sakyo-ku, Kyoto, 606-8507, Japan.

[3]The Hakubi Center for Advanced Research, Kyoto University, Yoshida-honmachi, Sakyo-ku, Kyoto-shi, Kyoto, 606-8501, Japan.

[4]Laboratory of Protein Metabolism, Tokyo Metropolitan Institute of Medical Science, 2-1-6 Kamikitazawa, Setagaya-ku, Tokyo 156-8506, Japan.

[5]Institute for Advanced Life Sciences, Hoshi University, 2-4-41 Ebara, Shinagawa-ku, Tokyo 142-8501, Japan.

[6]Corresponding author.

*E-mail: kiwai@mcp.med.kyoto-u.ac.jp

Abstract

The linear ubiquitin chain assembly complex (LUBAC), which consists of HOIP, SHARPIN, and HOIL-1L, promotes NF-κB activation and protects against cell death by generating linear ubiquitin chains. LUBAC contains two RING-IBR-RING (RBR) ubiquitin ligases (E3); the HOIP RBR is responsible for catalyzing linear ubiquitination. We found that HOIL-1L RBR plays a crucial role in LUBAC regulation. HOIL-1L RBR conjugates mono-ubiquitin onto all LUBAC subunits, followed by HOIP-mediated conjugation of linear chains onto mono-ubiquitin; these linear chains attenuate LUBAC functions. Introduction of E3-defective HOIL-1L mutants augmented linear ubiquitination, thereby protecting cells against *Salmonella* infection and curing dermatitis caused by reduction in LUBAC levels due to loss of SHARPIN. Our results reveal a regulatory mode of E3s in which the accessory E3 in LUBAC down-regulates the main E3 by providing preferred substrates for auto-linear ubiquitination. Thus, inhibition of HOIL-1L E3 represents a promising strategy for treating severe infections or immunodeficiency.

Text

The ubiquitin system, which is involved in the regulation of various physiological processes[1-6], requires the sequential transfer of ubiquitin by three enzymes: a ubiquitin-activating enzyme (E1), a ubiquitin-conjugating enzyme (E2), and a ubiquitin ligase (E3)[1,7]. The most important feature of the ubiquitin system is that ubiquitin, a small post-translational protein modifier, can be attached not only to its substrates, but also to other ubiquitin molecules, thereby generating ubiquitin chains. Several types of ubiquitin chains exist, and chain type determines the mode of regulation of conjugated proteins[1,7]. Previous work showed that ubiquitin chains are added to one of seven Lys (K) residues in ubiquitin[1,7]. However, recent work by our group revealed that a ubiquitin chain can also be generated via the N-terminal Met-1 (M1) of ubiquitin, yielding a linear or M1-linked ubiquitin chain, and that the linear ubiquitin assembly complex (LUBAC) specifically generates such linear chains[8-10]. LUBAC is composed of three subunits: HOIP, HOIL-1L, and SHARPIN; the RING-IBR-RING (RBR) of HOIP is the catalytic center for linear ubiquitination[9,10]. It has been recently shown that linear ubiquitin chains conjugated onto LUBAC subunits attenuate the linear ubiquitination activity of HOIP, and OTULIN, a linear chain-specific deubiquitinase (DUB) that interacts with LUBAC[11-13], counteracts this effect by cleaving the chains on LUBAC[14].

LUBAC contributes to NF-κB activation and protects against cell death by generating linear ubiquitin chains[8-10,15,16]. Promotion of linear ubiquitination is associated with oncogenesis, whereas attenuation of the process is associated with autoinflammation and immunodeficiency[17-21]. Moreover, pathogens such as *Salmonella*, *Shigella*, and

61 opportunistic *Aspergillus* inhibit LUBAC to promote infection[22-26].

62 LUBAC has two distinct RBR-type ubiquitin ligase activities, one each in
63 HOIP and HOIL-1L, within one ubiquitin ligase complex[9,10]. The HOIP RBR, as the main
64 catalytic center of LUBAC, specifically generates linear chains. Despite its relatively
65 weak E3 activity[27], HOIL-1L RBR has been suggested to be involved in linear
66 ubiquitination of NEMO by HOIP RBR[28]; however, LUBAC lacking this region can still
67 conjugate linear chains to NEMO[29]. Thus, the HOIL-1L E3 activity may have roles
68 besides NEMO ubiquitination. HOIL-1L catalyzes oxy-ester bond formation between the
69 C-terminal carboxyl group of ubiquitin and the hydroxy groups of Ser/Thr residues of
70 HOIL-1L and components of the Myddosome[30,31]. However, the physiological
71 significance of the second ligase of HOIL-1L within LUBAC remains elusive.

72 Here, we show that the E3 activity of HOIL-1L plays a crucial role in LUBAC
73 regulation. HOIL-1L E3 conjugates mono-ubiquitin onto all LUBAC subunits, followed
74 by HOIP E3–mediated conjugation of linear chains onto the mono-ubiquitin. We found
75 that introduction of a HOIL-1L mutant lacking E3 activity protected cells from
76 *Salmonella* infection by augmenting linear ubiquitination by LUBAC. More importantly,
77 introduction of even one E3-defective HOIL-1L allele dramatically cured dermatitis
78 caused by loss of SHARPIN[29,32]. These observations reveal a regulatory mode of E3, in
79 which the second, minor ligase activity of an E3 complex negatively regulates the main
80 ligase, and a ligase-associated DUB counteracts this effect. Our results also imply that
81 inhibition of HOIL-1L E3 activity represents a promising strategy for the treatment of
82 severe infections or immunodeficiency.

Results

The HOIL-1L E3 activity down-regulates LUBAC functions

The trimeric LUBAC E3 complex contains two catalytic RBR centers (Fig. 1a), and HOIL-1L RBR is highly conserved throughout evolution (Extended Data Fig. 1a). To investigate the functions of HOIL-1L E3, we introduced HOIL-1L WT or mutants lacking the HOIL-1L RBR, along with HOIP, into mouse embryonic fibroblasts (MEFs) lacking all LUBAC subunits (triple knockout [TKO] MEFs)[16]. The HOIL-1L mutants efficiently suppressed activation of caspase-3 triggered by TNF-α and cycloheximide (CHX) (Extended Data Fig. 1b). Cys458 of mouse HOIL-1L forms a thio-ester bond with ubiquitin prior to substrate ubiquitination[19,27,33]. Ligase-defective HOIL-1L harboring a mutation of Cys458 (C458S or C458A) suppressed caspase-3 activation and protected TKO MEFs from TNF-α–induced cell death (Fig. 1b,c, Extended Data Fig. 1c). Conjugation of linear chains to components of TNFR Complex I, including RIPK1, suppressed cell death by inhibiting formation of the TNF-α–mediated cell death complex containing RIPK1, FADD, and RIPK3 (TNFR Complex II)[34-36]. Consistent with this, loss of HOIL-1L E3 drastically suppressed generation of TNFR Complex II (Fig. 1d). Luciferase assays revealed that ligase-defective HOIL-1L activated NF-κB to a greater extent than WT (Extended Data Fig. 1d). Transcription of NF-κB target genes was strongly activated in MEFs expressing the ligase-defective HOIL-1L C458A mutant (Fig. 1e, Extended Data Fig. 1e). Moreover, phosphorylation and degradation of IκBα, a hallmark of NF-κB activation, was augmented even in the absence of stimulation (Fig. 1f, Extended Data Fig. 1f). Notably in this regard, HOIP-mediated linear ubiquitination

105 is involved in suppression of cell death by HOIL-1L RBR, as HOIL-1L C458S failed to
106 inhibit apoptosis of MEFs expressing the ligase-defective HOIP C879A mutant (Fig. 1g).
107
108 **HOIL-1L E3 attenuates generation of linear ubiquitin chains**
109 Because augmentation of LUBAC function upon loss of HOIL-1L E3 activity depended
110 on HOIP E3, we investigated whether loss of HOIL-1L E3 would affect the amount of
111 linear ubiquitin chains in cells. As expected, introduction of ligase-defective HOIL-1L
112 along with HOIP and SHARPIN dramatically increased the cellular level of linear
113 ubiquitin chains without affecting K48, K63, or other types of chains (Fig. 2a, Extended
114 Data Fig. 2a,b). Consistent with this, LUBAC immunoprecipitated from MEFs
115 expressing ligase-defective HOIL-1L generated more linear chains *in vitro* than LUBAC
116 containing HOIL-1L WT (Fig. 2b). Linear ubiquitination of NEMO, which is involved in
117 NF-κB activation[15,37], was also augmented in non-stimulated TKO MEFs expressing
118 HOIL-1L C458A (Fig. 2c). In addition, the amount of linear ubiquitin, as well as
119 ubiquitinated RIPK1, which is required for protection against cell death, was increased
120 by loss of HOIL-1L E3 (Fig. 2d). These results clearly demonstrated that HOIL-1L E3
121 down-regulated linear ubiquitination of known substrates, leading to suppression of
122 LUBAC functions, i.e., NF-κB activation and protection against cell death.
123
124 **Auto-ubiquitination of HOIL-1L inhibits LUBAC functions, including generation of**
125 **linear ubiquitin chains**

During our analyses of ligase-defective HOIL-1L, we realized that slowly migrating HOIL-1L was absent in cells lacking HOIL-1L E3 activity (Fig. 2a,c). The upper HOIL-1L signal appeared to represent auto-ubiquitinated HOIL-1L, as this band was observed in cells lacking HOIP E3 activity[38] (Extended Data Fig. 3a). *In vitro* ubiquitination assays confirmed that HOIL-1L auto-monoubiquitinates itself (Fig. 3a). It was recently reported that HOIL-1L can catalyze oxy-ester bond formation between itself and ubiquitin[30,31]. This oxy-ester bond was cleaved by hydroxylamine (NH_2OH) treatment, but not a DUB, Ub-Specific Protease2 (USP2cc), which cleaves all conventional ubiquitin conjugations[31] (Extended Data Fig. 3b). Isopeptide linkages between Lys residues in substrates and ubiquitin are cleaved by USP2cc, but not NH_2OH[31]. To our surprise, a substantial amount of ubiquitinated HOIL-1L (Ub-HOIL-1L) generated by HOIL-1L E3 *in vitro* was resistant to NH_2OH but could be digested by USP2cc (Fig. 3b), indicating that most Ub-HOIL-1L is generated via Lys residues. As previously observed[31], however, USP2cc failed to eliminate slower-migrating HOIL-1L immunoprecipitated under non-denatured conditions (Fig. 3c). Because the upper HOIL-1L signal was not detected in MEFs lacking SHARPIN, which contain LUBAC consisting of HOIL-1L and HOIP (Extended Data Fig. 3c), we suspected that USP2cc failed to access ubiquitin in the tight trimeric LUBAC complex[16]. To test this possibility, we immunoprecipitated HOIL-1L under denaturing conditions to disrupt the LUBAC complex. USP2cc, but not the linear-specific DUB OTULIN, could efficiently, albeit not completely, eliminate the slower-migrating HOIL-1L immunoprecipitated under denaturing conditions (Fig. 3c). Also, NH_2OH marginally cleaved Ub-HOIL-1L (Extended Data Fig. 3d). We then examined the

148 ubiquitinated residues by mass spectrometry (MS). These analyses identified Lys residues
149 of HOIP, HOIL-1L, and SHARPIN as residues ubiquitinated in cells expressing HOIL-
150 1L WT. In addition, S107 of human HOIP was identified as ubiquitinated in cells
151 expressing HOIL-1L WT, but not the ligase-defective HOIL-1L C460A mutant
152 (Extended Data Fig. 3e). The MS results strongly indicated that a substantial fraction of
153 Ub-HOIL-1L in cells is generated via Lys residues, whereas oxy-ester ubiquitination also
154 occurs in cells expressing HOIL-1L WT although we could not detect ubiquitinated
155 serine/threonine (S/T) in HOIL-1L.

156 Hence, we focused on the Lys residues of HOIL-1L. K158 and K174 of mouse
157 HOIL-1L (mHOIL-1L) were identified as ubiquitinated residues in MS analyses[39].
158 However, HOIL-1L mutants in which K158 and K174 were replaced with Arg
159 (K158/174R), as well as other mono-K/R mutants, were mono-ubiquitinated (Extended
160 Data Fig. 3f). We then modified all 17 Lys residues of mHOIL-1L to Arg (All-K/R) and
161 found that the resultant HOIL-1L All-K/R mutant was barely ubiquitinated (Fig. 3d).
162 Moreover, the All-K/R mutant increased the level of linear ubiquitin chains in the cell,
163 promoted NF-κB activation, and protected MEFs against TNF-α–induced apoptosis (Fig.
164 3e,f, Extended Data Fig. 3g). Introduction of a 3×FLAG-tag (3×FLAG–HOIL-1L All-
165 K/R), but not a myc-tag, at the N-terminus enabled HOIL-1L All-K/R to auto-ubiquitinate
166 (Fig. 3g, Extended Data Fig. 3h). A Lys residue in the 3×FLAG-tag was ubiquitinated,
167 and as expected the ubiquitin on that residue was effectively cleaved by USP2cc, but not
168 NH_2OH (Fig. 3h, Extended Data Fig. 3i). However, we could not detect a ubiquitinated
169 signal in the myc-tag. Given that 3×FLAG–HOIL-1L All-K/R C458A did not

ubiquitinate HOIL-1L (Fig. 3g), HOIL-1L All-K/R must have auto-ubiquitinated Lys residues in the N-terminal 3×FLAG-tag on its own. In MS analyses, we could detect ubiquitination of S915 and T955 of mHOIP in HOIL-1L All-K/R cells, implying that the All-K/R mutations did not overtly affect HOIL-1L function (Extended Data Fig. 3j,k). Moreover, introduction of the N-terminal 3×FLAG-tag reversed the increase in linear chain production and the suppression of TNF-α–mediated apoptosis induced by All-K/R, but not the corresponding effects of the ligase-defective mutant (Fig. 3i, Extended Data Fig. 3l). Although we cannot rule out the possibility that loss of mono-ubiquitination or the All-K/R mutations may alter conformation of the LUBAC complex to augment the E3 activity of HOIP completely, these results clearly indicated that auto-ubiquitination of HOIL-1L suppresses LUBAC functions, regardless of the positions of the ubiquitinated residues.

Auto-mono–ubiquitination makes HOIL-1L a preferred target for auto-linear ubiquitination by HOIP

To dissect the molecular mechanism underlying the suppression of linear ubiquitination by LUBAC mediated by auto-ubiquitination of HOIL-1L, we performed *in vitro* ubiquitination assays. Petit-SHARPIN, which consists of fragments of human HOIP (hHOIP) and hSHARPIN, has weak linear ubiquitination activity (Fig. 4a)[23]. Addition of mHOIL-1L augmented the linear ubiquitination activity of Petit-SHARPIN, confirming that trimeric LUBAC has efficient linear ubiquitination activity[29] (Fig. 4b). Addition of not only ligase-defective mHOIL-1L (C458A) or hHOIL-1L (C460A), but also HOIL-1L

All-K/R, potentiated activity to a greater extent than mHOIL-1L WT (Fig. 4b,c, Extended Data Fig. 4a). Because HOIL-1L C458A was linearly ubiquitinated to a lesser extent than WT (Extended Data Fig. 4b), we generated ligase-defective HOIL-1L with ubiquitin at the N-terminus (Ub-HOIL-1L ΔE3). Addition of ubiquitin reversed HOIL-1L ΔE3–mediated potentiation of linear ubiquitination, and Ub-HOIL-1L ΔE3 was efficiently linearly ubiquitinated (Fig. 4d). These results clearly demonstrated that auto-ubiquitination of HOIL-1L attenuates linear ubiquitination by HOIP E3 by making HOIL-1L a preferred substrate for HOIP RBR. Moreover, addition of Petit-SHARPIN C885A (which lacks linear ubiquitination activity) to HOIL-1L strengthened the auto-ubiquitination activity of HOIL-1L (Fig. 4e), suggesting that formation of trimeric LUBAC also potentiates HOIL-1L E3 activity.

Not only HOIL-1L, but also HOIP and SHARPIN, are mono-ubiquitinated by HOIL-1L E3

OTULIN maintains LUBAC functions by cleaving linear chains conjugated to LUBAC subunits, including HOIP[14]. We found that loss of OTULIN increased the levels of slower-migrating bands corresponding to all three components of LUBAC in cells expressing HOIL-1L WT, but not HOIL-1L C458A (Fig. 5a). Modifications of LUBAC subunits in OTULIN KO cells appeared to be linear chains, as all three subunits of LUBAC were efficiently pulled down with M1-TUBE, which selectively binds linear ubiquitin chains (Fig. 5b). OTULIN cleaves only inter-ubiquitin linear linkages, but not ubiquitin-substrate bonds. Treatment of OTULIN KO cells with MBP-OTULIN

increased the levels of mono-ubiquitinated species (Extended Data Fig. 5a), strongly indicating the involvement of HOIL-1L E3 in linear ubiquitination of all LUBAC subunits. Indeed, *in vitro* ubiquitination assays clearly confirmed that HOIL-1L, but not ligase-defective HOIL-1L, mono-ubiquitinated all subunits of LUBAC (Fig. 5c).

RBR E3s bind to E2 at RING1 and transfer ubiquitin from E2 to the conserved Cys in RING2 prior to substrate ubiquitination[19,40-42]. We generated a HOIL-1L mutant lacking amino acids 251–341, the region containing RING1 (ΔRING1) (Extended Data Fig. 5b). Although all LUBAC subunits were linearly ubiquitinated in cells lacking OTULIN, expression of HOIL-1L ΔRING1 counteracted the increase in their linear ubiquitination induced by OTULIN deletion, implying that E2 bound to HOIL-1L RING1 transfers ubiquitin to HOIL-1L C458 (Fig. 5d, e). Consistent with this, HOIL-1L ΔRING1 or C458A attenuated the augmentation of TNF-α–induced apoptosis induced by OTULIN deletion (Fig.5 f,g, Extended Data Fig. 5c). These results reveal the molecular mechanism underlying HOIL-1L–mediated suppression of LUBAC functions: HOIL-1L E3 mono-ubiquitinates not only HOIL-1L itself but also HOIP and SHARPIN, thereby facilitating HOIP-mediated conjugation of linear chains to all LUBAC subunits by providing a suitable substrate (i.e., acceptor ubiquitin) for HOIP RBR[33]. As demonstrated previously[14], this leads to suppression of LUBAC functions. OTULIN counteracts these effects by cleaving linear chains from the LUBAC complex. Considering that loss of HOIL-1L E3 increased the level of linear chains in the cell (Fig. 2a), HOIL-1L E3 may cause HOIP RBR to preferentially recognize LUBAC itself as cis-targets over other substrates (trans-

targets) for linear chain conjugation, thereby contributing to suppression of LUBAC functions. (Fig. 5h).

Defective HOIL-1L E3 activity protects cells against *Salmonella typhimurium* infections

We next examined the pathophysiological impacts of HOIL-1L E3. LUBAC protects cells against infection by invasive bacteria, including *Salmonella*[22,24]. Loss of HOIL-1L E3 efficiently restricted proliferation of *S. typhimurium*, as well as infection-induced cell death (Fig. 6a-c, Extended Data Fig. 6a). Structured illumination microscopy (SIM) revealed that infecting *S. typhimurium* were covered with high levels of linear ubiquitin (Fig. 6d, Extended Data Fig. 6b–d). Moreover, infection strongly induced expression of NF-κB target genes in MEFs expressing HOIL-1L C458A (Fig. 6e). Considering that the levels of LUBAC subunits were virtually identical between MEFs expressing WT and HOIL-1L C458A (Fig. 2a–d), we concluded that loss of HOIL-1L E3 augmented LUBAC activity, resulting in effective clearance of *S. typhimurium*.

Loss of HOIL-1L E3 protects mice from apoptotic liver failure and cures dermatitis caused by lack of SHARPIN

HOIL-1L ΔRING1 augmented NF-κB activation, suppressed apoptosis, and generated linear ubiquitin chains at a level comparable to the C458A mutant (Extended Data Fig. 7a–d). Hence, to examine the effects of HOIL-1L E3 knockout in mice, we generated conditional knockout (KO) mice in which exons 7 and 8 of HOIL-1L (which encode

257 amino acids 251–341) were deleted (ΔRING1) (Extended Data Fig. 5b, 7e). Expression
258 levels of HOIL-1L ΔRING1 were relatively low, whereas the levels of the other
259 components of LUBAC were almost the same as in WT (Extended Data Fig. 7f). HOIL-
260 1L can exist alone without forming LUBAC[29]. Anti-SHARPIN immunoprecipitation
261 revealed that almost all HOIL-1L ΔRING1 formed a complex with SHARPIN and HOIP,
262 whereas a substantial amount of HOIL-1L WT was not present in LUBAC and could be
263 detected in the unbound fraction (Extended Data Fig. 7g). Accordingly, we used HOIL-
264 1L ΔRING1 for subsequent analyses because deletion of RING1 did not overtly affect the
265 amount of LUBAC, although catalytic inactive point-mutation (C458A) might be
266 preferred to delete HOIL-1L E3 activity. Mice with whole-body deletion of HOIL-1L
267 RING1 (HOIL-1L$^{\Delta RING1/\Delta RING1}$) were viable up to the age of 12 months without overt
268 phenotypes (Fig. 7a), although loss of HOIL-1L E3 significantly increased the amount of
269 linear ubiquitin in all organs (Fig. 7b, Extended Data Fig. 7h). Immunostaining revealed
270 linear chains in lung tissue, indicating that LUBAC functions were augmented in HOIL-
271 1L$^{\Delta RING1/\Delta RING1}$ mice (Fig. 7c). However, HOIL-1L ΔRING1 mice did exhibit some mild
272 phenotypes. For example, the mice exhibited mild splenomegaly; infiltration by
273 inflammatory cells in most organs, especially the lungs; and elevated serum levels of
274 immunoglobulin (Fig. 7d–f). Moreover, flow cytometry revealed that the percentage of
275 activated B cells and CD4^{+} T cells increased (Fig. 7g,h, Extended Data Fig. 7i).

276 HOIL-1L$^{\Delta RING1/\Delta RING1}$ MEFs and primary hepatocytes were resistant to TNF-
277 α–induced apoptosis (Extended Data Fig. 8a–c). Hence, we examined the effects of loss
278 of HOIL-1L E3 in disease models. Intraperitoneal injection of lipopolysaccharide (LPS)

279 and D-galactosamine (D-GalN), a specific inhibitor of hepatic transcription, induces
280 acute hepatocytic apoptosis[43,44]; we investigated whether loss of HOIL-1L E3 would
281 protect mice against this effect. Although we observed no apparent differences in livers
282 not injected with LPS/D-GalN (Extended Data Fig. 8d), LPS and D-GalN induced
283 massive hepatocyte apoptosis in WT livers 7 hours after injection, whereas virtually no
284 overt apoptosis could be detected in HOIL-1L$^{\Delta RING1/\Delta RING1}$ livers (Fig. 8a, Extended Data
285 Fig. 8e,f). Loss of HOIL-1L E3 also protected mice from death triggered by LPS/D-GalN
286 injection (Fig. 8b). These results indicated that deletion of HOIL-1L E3 protects against
287 apoptotic cell death.

288 Loss of SHARPIN causes chronic autoinflammation in the skin (chronic
289 proliferative dermatitis in mice: cpdm) due to augmented TNF-α–induced death of
290 keratinocytes, a result of the decrease in LUBAC ligase activity caused by reduced levels
291 of HOIL-1L and HOIP[29,32,45]. To increase LUBAC activity in cpdm mice, we introduced
292 the HOIL-1L$^{\Delta RING1}$ alleles. To our great surprise, introduction of even one HOIL-1L$^{\Delta RING1}$
293 allele dramatically ameliorated cpdm dermatitis and suppressed keratinocyte apoptosis
294 without affecting the amount of HOIP (Fig. 8c–e, Extended Data Fig. 8 g,h). These results
295 clearly show that augmentation of linear ubiquitination activity of HOIP E3 upon loss of
296 HOIL-1L E3 ameliorates cpdm. Moreover, the findings indicate that cpdm is caused
297 mainly by attenuated HOIP E3 activity rather than altered composition of LUBAC
298 subunits.
299

Discussion

The LUBAC ubiquitin ligase complex promotes NF-κB activation and suppresses cell death by conjugating linear ubiquitin chains[9,10]. Experiments involving deletion or mutation of OTULIN have revealed that LUBAC conjugates linear ubiquitin chains to its subunits, thereby down-regulating its own functions[14]. LUBAC contains two ubiquitin ligase centers, the RBRs of HOIP and HOIL-1L; the former catalyzes formation of linear ubiquitin chains[8,9]. In this study, over the course of our analyses for HOIL-1L RBR, we identified an unexpected regulatory mode of the LUBAC ubiquitin ligase, in which two different E3s work coordinately to regulate LUBAC functions (Fig. 5h). The accessory E3 center HOIL-1L RBR mono-ubiquitinates LUBAC subunits, which makes the subunits preferred auto-linear ubiquitination (cis-linear ubiquitination) substrates for the main E3 of LUBAC, HOIP RBR, thereby suppressing linear chain-mediated LUBAC functions by attenuating linear ubiquitination of other targets (trans-linear ubiquitination). Notably, since ubiquitin is the preferred target of linear ubiquitination by HOIP E3[46], loss of auto-mono-ubiquitination activity of HOIL-1L E3 renders LUBAC subunits undesirable substrates for linear ubiquitination by HOIP RBR. Therefore, HOIL-1L ΔRING1 or the C458A mutant leads to enhancement, but not suppression, of LUBAC function, which underlies the benign phenotype of mice lacking E3 activity of HOIL-1L as compared to the HOIL-1L null mice and the reversal of the SHARPIN null phenotype by the HOIL-1L ΔRING1. OTULIN counteracts it by digesting linear chains from LUBAC, which are conjugated by coordinating function of HOIL-1L and HOIP E3s, via a process that depends on a constitutive interaction between the deubiquitinase and the

complex[14]. Coordination between the functions of two different E3s has been reported previously; however, in those cases, the first E3 mono-ubiquitinates the target proteins, and the second E3 polyubiquitinates the mono-ubiquitin residues introduced by the first to efficiently conjugate ubiquitin chains to substrates[47,48]. By contrast, in the case of LUBAC, the coordinate functions of two E3s regulate the main catalytic activity by decorating the ligase complex itself, and two E3s, HOIL-1L and HOIP, are present in the same ligase complex.

We also provided solid evidence that deletion of HOIL-1L E3 potentiates LUBAC functions *in vitro* and *in vivo*. Augmented LUBAC activity has been implicated in lymphomagenesis[18,49] and resistance to chemotherapeutic agents such as cisplatin[50,51]. The MALT1 paracaspase, which removes HOIL-1L RBR from LUBAC by cleaving HOIL-1L between Arg165 and Gly166[52,53], is upregulated in most activated B cell-like diffuse large B cell lymphoma (ABC-DLBCL)[53,54]. Although it was suggested that MALT1-mediated cleavage of HOIL-1L suppresses LUBAC functions[52], we have observed that the HOIL-1L 'before NZF' mutant, which resembles HOIL-1L (1–165), augmented LUBAC function (Extended Data Fig. 1b). Because augmented LUBAC activity is involved in the pathogenesis of ABC-DLBCL[18], MALT1-mediated cleavage of HOIL-1L may augment the function of LUBAC, which plays critical roles in lymphomagenesis. Although HOIL-1L mutations play causative roles in diseases associated with suppressed LUBAC functions[21,55-57], our results imply that some mutations in HOIL-1L may augment LUBAC activity by suppressing HOIL-1L E3. Given that loss of even one allele of HOIL-1L RING1 can augment LUBAC function in

mice sufficiently to cure cpdm (Fig. 8c), some HOIL-1L mutations may be involved in oncogenesis by augmenting LUBAC function. Further analyses of cancer genomes will reveal whether or not HOIL-1L mutations are involved in oncogenesis. Pathogens such *Shigella* and opportunistic *Aspergillus* inhibit LUBAC to promote infection[23,26]. Here, we showed that inhibition of HOIL-1L E3 augmented clearance of the intracellular pathogen *Salmonella* (Fig. 6). Thus, our results identify HOIL-1L E3 as a promising target for potentiating clearance of pathogens, especially in immunocompromised hosts.

Acknowledgments

We thank Drs. Y. Takeda, T Jo and Y. Sasaki for insightful discussion, Dr. T. Nakagawa and J. Matsuhiro for protein purification, Y. Sugahara and Y. Hayamizu for animal care, and N. Ueno for technical assistance. This study was supported by JSPS KAKENHI Grant Numbers 24112002, 25253019, JP17H06174, and JP18H05499 (to K.I.); JSPS KAKENHI Grant Number JP17K08786, a Grant for Joint Research Project of the Institute of Medical Science from the University of Tokyo, and the Hakubi-project grant, Kyoto University (to M.K.); and JSPS KAKENHI Grant Number JP18H05498 (to F.O.).

Author Contributions

Y.F., H.F., and K.I. conceived and designed the project. Y.F. performed most of the experiments. M.K. and A.N. performed bacterial infection experiments. F.O., Y.S., and K.T. performed mass spectrometry. K.S. performed immunostaining of lungs of mice and generation of M1-TUBE. R.T. provided advice on the project. Y.F. and K.I. wrote the manuscript with contributions from all other authors.

Competing Financial Interests

The authors declare no competing financial interests.

370 REFERENCES

371 1. Hershko, A. & Ciechanover, A. The ubiquitin system. *Annu. Rev. Biochem.* **67**,
372 425-479 (1998).
373 2. Komander, D. & Rape, M. The ubiquitin code. *Annu. Rev. Biochem.* **81**, 203-229
374 (2012).
375 3. Husnjak, K. & Dikic, I. Ubiquitin-binding proteins: decoders of ubiquitin-
376 mediated cellular functions. *Annu. Rev. Biochem.* **81**, 291-322 (2012).
377 4. Mukhopadhyay, D. & Riezman, H. Proteasome-independent functions of
378 ubiquitin in endocytosis and signaling. *Science* **315**, 201-205 (2007).
379 5. Wickliffe, K., Williamson, A., Jin, L. & Rape, M. The multiple layers of ubiquitin-
380 dependent cell cycle control. *Chem. Rev.* **109**, 1537-1548 (2009).
381 6. Zinngrebe, J., Montinaro, A., Peltzer, N. & Walczak, H. Ubiquitin in the immune
382 system. *EMBO Rep.* **15**, 28-45 (2014).
383 7. Kornitzer, D. & Ciechanover, A. Modes of regulation of ubiquitin-mediated
384 protein degradation. *J. Cell Physiol.* **182**, 1-11 (2000).
385 8. Kirisako, T. *et al.* A ubiquitin ligase complex assembles linear polyubiquitin
386 chains. *EMBO J.* **25**, 4877-4887 (2006).
387 9. Iwai, K., Fujita, H. & Sasaki, Y. Linear ubiquitin chains: NF-κB signalling, cell
388 death and beyond. *Nat. Rev. Mol. Cell Biol.* **15**, 503-508 (2014).
389 10. Sasaki, K. & Iwai, K. Roles of linear ubiquitinylation, a crucial regulator of NF-
390 κB and cell death, in the immune system. *Immunol. Rev.* **266**, 175-189 (2015).
391 11. Takiuchi, T. *et al.* Suppression of LUBAC-mediated linear ubiquitination by a
392 specific interaction between LUBAC and the deubiquitinases CYLD and
393 OTULIN. *Genes Cells* **19**, 254-272 (2014).
394 12. Damgaard, R.B. *et al.* The Deubiquitinase OTULIN Is an Essential Negative
395 Regulator of Inflammation and Autoimmunity. *Cell* **166**, 1215-1230 e1220 (2016).
396 13. Elliott, P.R. & Komander, D. Regulation of Met1-linked polyubiquitin signalling
397 by the deubiquitinase OTULIN. *FEBS J.* **283**, 39-53 (2016).
398 14. Heger, K. *et al.* OTULIN limits cell death and inflammation by deubiquitinating
399 LUBAC. *Nature* **559**, 120-124 (2018).
400 15. Fujita, H. *et al.* Mechanism underlying IκB kinase activation mediated by the
401 linear ubiquitin chain assembly complex. *Mol. Cell. Biol.* **34**, 1322-1335 (2014).

16. Fujita, H. *et al.* Cooperative Domain Formation by Homologous Motifs in HOIL-1L and SHARPIN Plays A Crucial Role in LUBAC Stabilization. *Cell Rep.* **23**, 1192-1204 (2018).
17. Boisson, B. *et al.* Human HOIP and LUBAC deficiency underlies autoinflammation, immunodeficiency, amylopectinosis, and lymphangiectasia. *J. Exp. Med.* **212**, 939-951 (2015).
18. Yang, Y. *et al.* Essential role of the linear ubiquitin chain assembly complex in lymphoma revealed by rare germline polymorphisms. *Cancer Discov.* **4**, 480-493 (2014).
19. Elton, L., Carpentier, I., Verhelst, K., Staal, J. & Beyaert, R. The multifaceted role of the E3 ubiquitin ligase HOIL-1: beyond linear ubiquitination. *Immunol. Rev.* **266**, 208-221 (2015).
20. Brazee, P., Dada, L.A. & Sznajder, J.I. Role of Linear Ubiquitination in Health and Disease. *Am. J. Respi.r Cell Mol. Biol.* **54**, 761-768 (2016).
21. Boisson, B. *et al.* Immunodeficiency, autoinflammation and amylopectinosis in humans with inherited HOIL-1 and LUBAC deficiency. *Nat. Immunol.* **13**, 1178-1186 (2012).
22. Noad, J. *et al.* LUBAC-synthesized linear ubiquitin chains restrict cytosol-invading bacteria by activating autophagy and NF-κB. *Nat. Microbiol.* **2**, 17063 (2017).
23. Sakamoto, H. *et al.* Gliotoxin suppresses NF-κB activation by selectively inhibiting linear ubiquitin chain assembly complex (LUBAC). *ACS. Chem. Biol.* **10**, 675-681 (2015).
24. van Wijk, S.J.L. *et al.* Linear ubiquitination of cytosolic Salmonella Typhimurium activates NF-κB and restricts bacterial proliferation. *Nat. Microbiol.* **2**, 17066 (2017).
25. MacDuff, D.A. *et al.* Phenotypic complementation of genetic immunodeficiency by chronic herpesvirus infection. *Elife* **4** (2015).
26. de Jong, M.F., Liu, Z., Chen, D. & Alto, N.M. Shigella flexneri suppresses NF-κB activation by inhibiting linear ubiquitin chain ligation. *Nat. Microbiol.* **1**, 16084 (2016).
27. Stieglitz, B., Morris-Davies, A.C., Koliopoulos, M.G., Christodoulou, E. & Rittinger, K. LUBAC synthesizes linear ubiquitin chains via a thioester

intermediate. *EMBO Rep.* **13**, 840-846 (2012).

28. Smit, J.J. *et al.* Target specificity of the E3 ligase LUBAC for ubiquitin and NEMO relies on different minimal requirements. *J. Biol Chem* **288**, 31728-31737 (2013).

29. Tokunaga, F. *et al.* SHARPIN is a component of the NF-κB-activating linear ubiquitin chain assembly complex. *Nature* **471**, 633-636 (2011).

30. Cohen, P., Kelsall, I.R., Nanda, S.K. & Zhang, J. HOIL-1, an atypical E3 ligase that controls MyD88 signalling by forming ester bonds between ubiquitin and components of the Myddosome. *Adv. Biol. Regul*, 100666 (2019).

31. Kelsall, I.R., Zhang, J., Knebel, A., Arthur, J.S.C. & Cohen, P. The E3 ligase HOIL-1 catalyses ester bond formation between ubiquitin and components of the Myddosome in mammalian cells. *Proc. Natl. Acad. Sci. U S A* **116**, 13293-13298 (2019).

32. Ikeda, F. *et al.* SHARPIN forms a linear ubiquitin ligase complex regulating NF-κB activity and apoptosis. *Nature* **471**, 637-641 (2011).

33. Dove, K.K. & Klevit, R.E. RING-Between-RING E3 Ligases: Emerging Themes amid the Variations. *J. Mol. Biol.* **429**, 3363-3375 (2017).

34. Peltzer, N., Darding, M. & Walczak, H. Holding RIPK1 on the Ubiquitin Leash in TNFR1 Signaling. *Trends Cell Biol.* **26**, 445-461 (2016).

35. Ting, A.T. & Bertrand, M.J.M. More to Life than NF-kappaB in TNFR1 Signaling. *Trends Immunol.* **37**, 535-545 (2016).

36. Wertz, I.E. *et al.* Phosphorylation and linear ubiquitin direct A20 inhibition of inflammation. *Nature* **528**, 370-375 (2015).

37. Tokunaga, F. *et al.* Involvement of linear polyubiquitylation of NEMO in NF-κB activation. *Nat. Cell Biol.* **11**, 123-132 (2009).

38. Peltzer, N. *et al.* HOIP deficiency causes embryonic lethality by aberrant TNFR1-mediated endothelial cell death. *Cell Rep.* **9**, 153-165 (2014).

39. Kim, W. *et al.* Systematic and quantitative assessment of the ubiquitin-modified proteome. *Mol. Cell* **44**, 325-340 (2011).

40. Reiter, K.H. & Klevit, R.E. Characterization of RING-Between-RING E3 Ubiquitin Transfer Mechanisms. *Methods Mol. Biol.* **1844**, 3-17 (2018).

41. Walden, H. & Rittinger, K. RBR ligase-mediated ubiquitin transfer: a tale with many twists and turns. *Nat. Struct. Mol. Biol.* **25**, 440-445 (2018).

42. Dove, K.K. *et al.* Structural Studies of HHARI/UbcH7 approximately Ub Reveal Unique E2 approximately Ub Conformational Restriction by RBR RING1. *Structure* **25**, 890-900 e895 (2017).
43. Maes, M., Vinken, M. & Jaeschke, H. Experimental models of hepatotoxicity related to acute liver failure. *Toxicol. Appl. Pharmacol.* **290**, 86-97 (2016).
44. Mignon, A. *et al.* LPS challenge in D-galactosamine-sensitized mice accounts for caspase-dependent fulminant hepatitis, not for septic shock. *Am. J. Respir. Crit. Care. Med.* **159**, 1308-1315 (1999).
45. Kumari, S. *et al.* Sharpin prevents skin inflammation by inhibiting TNFR1-induced keratinocyte apoptosis. *Elife* **3** (2014).
46. Stieglitz, B. *et al.* Structural basis for ligase-specific conjugation of linear ubiquitin chains by HOIP. *Nature* **503**, 422-426 (2013).
47. Dove, K.K. *et al.* Two functionally distinct E2/E3 pairs coordinate sequential ubiquitination of a common substrate in Caenorhabditis elegans development. *Proc. Natl. Acad. Sci. U S A* **114**, E6576-E6584 (2017).
48. Scott, D.C. *et al.* Two Distinct Types of E3 Ligases Work in Unison to Regulate Substrate Ubiquitylation. *Cell* **166**, 1198-1214 e1124 (2016).
49. Dubois, S.M. *et al.* A catalytic-independent role for the LUBAC in NF-κB activation upon antigen receptor engagement and in lymphoma cells. *Blood* **123**, 2199-2203 (2014).
50. MacKay, C. *et al.* E3 ubiquitin ligase HOIP attenuates apoptotic cell death induced by cisplatin. *Cancer Res.* **74**, 2246-2257 (2014).
51. Niu, J., Shi, Y., Iwai, K. & Wu, Z.H. LUBAC regulates NF-κB activation upon genotoxic stress by promoting linear ubiquitination of NEMO. *EMBO J.* **30**, 3741-3753 (2011).
52. Klein, T. *et al.* The paracaspase MALT1 cleaves HOIL1 reducing linear ubiquitination by LUBAC to dampen lymphocyte NF-κB signalling. *Nat. Commun.* **6**, 8777 (2015).
53. Douanne, T., Gavard, J. & Bidere, N. The paracaspase MALT1 cleaves the LUBAC subunit HOIL1 during antigen receptor signaling. *J. Cell Sci.* **129**, 1775-1780 (2016).
54. Hailfinger, S. *et al.* Essential role of MALT1 protease activity in activated B cell-like diffuse large B-cell lymphoma. *Proc. Natl. Acad. Sci. U S A* **106**, 19946-

19951 (2009).

55. Wang, K. *et al.* Whole-genome DNA/RNA sequencing identifies truncating mutations in RBCK1 in a novel Mendelian disease with neuromuscular and cardiac involvement. *Genome Med.* **5**, 67 (2013).

56. Nilsson, J. *et al.* Polyglucosan body myopathy caused by defective ubiquitin ligase RBCK1. *Ann. Neurol.* **74**, 914-919 (2013).

57. Krenn, M. *et al.* Mutations outside the N-terminal part of RBCK1 may cause polyglucosan body myopathy with immunological dysfunction: expanding the genotype-phenotype spectrum. *J. Neurol.* **265**, 394-401 (2018).

512 **Figure Legends**

513 **Fig. 1 | HOIL-1L E3 activity negatively regulates LUBAC functions, including**
514 **suppression of apoptosis and NF-κB activation.**

515 **a**, Schematic representation of the domains of LUBAC subunits. **b, c,** Suppression of
516 apoptosis by ligase-defective HOIL-1L. **b,** Lysates from LUBAC TKO MEFs stably
517 reconstituted with the indicated proteins and stimulated with TNF-α (2.5 ng ml^{-1}) and
518 CHX (20 μg ml^{-1}) were probed as indicated. The experiments were repeated twice,
519 independently, with similar results. **c**, Cell death of the indicated MEFs following
520 treatment with TNF-α (10 ng ml^{-1}) and CHX (20 μg ml^{-1}) was monitored by assaying for
521 lactate dehydrogenase (LDH) activity. Mean ± S.D. is shown; n=3 independent
522 experiments. *P*-values are from one-way ANOVA. **d**, Generation of TNFR Complex II
523 (anti-FADD immunoprecipitates: IP) in MEFs stably expressing the indicated proteins.
524 The experiments were repeated twice, independently, with similar results. **e**, Expression
525 of NF-κB target genes, as determined by qPCR, in MEFs expressing the indicated
526 proteins. Mean ± S.D is shown; n=5 independent experiments; *P*-values are from two-
527 tailed Student's t-test. **f**, Phosphorylation and degradation of IκBα in LUBAC TKO
528 MEFs expressing the indicated proteins and treated with CHX (20 μg ml^{-1}). The
529 experiments were repeated three times, independently, with similar results. **g**, Caspase-3
530 cleavage in MEFs expressing the indicated proteins treated with TNF-α (2.5 ng ml^{-1}) and
531 CHX (20 μg ml^{-1}). The experiments were repeated three times, independently, with
532 similar results. Statistical source data are provided in Statistical Source Data Fig. 1 and
533 unprocessed immunoblots are provided in Unprocessed Blots Figure 1.

Fig. 2 | HOIL-1L E3 activity negatively regulates generation of linear ubiquitin chains by LUBAC.

a, Augmented generation of linear ubiquitin chains in HEK293T cells expressing ligase-defective HOIL-1L. Lysates from HEK293T cells transfected with the indicated expression plasmids were probed as indicated. **b**, Augmented linear ubiquitination by LUBAC containing ligase-defective HOIL-1L. LUBAC containing the indicated HOIL-1L proteins was immunoprecipitated from LUBAC TKO MEFs with anti-HA antibody. The samples were subjected to *in vitro* ubiquitination assays, and lysates of the cells were probed with the indicated antibodies. **c**, Linear ubiquitination in anti-NEMO immunoprecipitates from LUBAC TKO MEFs stably expressing the indicated proteins, not subjected to any stimulation. Cells were lysed with lysis buffer containing 10 mM N-ethylmaleimide (NEM). **d**, Linear ubiquitination and RIPK1 ubiquitination in anti-FLAG immunocomplexes from LUBAC TKO MEFs stably reconstituted with the indicated proteins, stimulated with FLAG-TNF-α for the indicated periods.

The data shown were repeated three times, independently, with similar results. Unprocessed immunoblots are provided in Unprocessed Blots Figure 2.

Fig. 3 | Auto-ubiquitination of HOIL-1L inhibits LUBAC functions by suppressing generation of linear ubiquitin chains.

a, Modification of HOIL-1L in the presence of indicated HOIL-1L proteins in *in vitro* ubiquitination assays, which were conducted at 37°C for the indicated times. **b,**

Generation of upper (modified) HOIL-1L signal in *in vitro* ubiquitination assays (37°C, 18 h), and digestion of the upper (modified) HOIL-1L signal generated *in vitro* with USP2cc or NH_2OH (37°C, 1 h). **c**, Digestion of the upper (modified) HOIL-1L signal with USP2cc or OTULIN (37°C, 1 h) in anti-FLAG immunoprecipitates obtained under non-denaturing or denaturing conditions from LUBAC TKO MEFs expressing 3×FLAG–HOIL-1L. The amount of modified HOIL-1L was assessed by immunoblotting (**a–c**). **d**, **e**, Upper HOIL-1L signal (**d**) and linear ubiquitin chains (**e**) in HEK293T cells expressing the indicated HOIL-1L proteins, as determined by immunoblotting. **f**, Caspase-3 cleavage in LUBAC TKO MEFs stably reconstituted with the indicated HOIL-1L proteins, stimulated with TNF-α (5 ng ml^{-1}) and CHX (20 μg ml^{-1}). **g,** LUBAC TKO MEFs stably expressing the indicated proteins were probed as indicated to estimate the amount of modified HOIL-1L. **h,** LUBAC TKO MEFs stably reconstituted with mHOIP, SHARPIN, and 3×FLAG-HOIL All-K/R were subjected to mass spectrometry to assess the ubiquitination sites in the 3×FLAG residues of HOIL All-K/R. **i**, Viability of LUBAC TKO MEFs expressing the indicated HOIL-1L proteins, stimulated with TNF-α (10 ng ml^{-1}), was evaluated using the iCELLigence system.

The data shown were repeated three times, independently, with similar results. Unprocessed immunoblots are provided in Unprocessed Blots Figure 3.

Fig. 4 | HOIL-1L E3 activity negatively regulates LUBAC functions *in vitro.*

a, Schematic representation of the domains of Petit-SHARPIN and experimental protocols for **b–e**. **b–d**, Generation of linear chains in the presence of the indicated HOIL-

578 1L proteins in *in vitro* ubiquitination assays of Petit-SHARPIN, as assessed by
579 immunoblotting with the indicated antibodies. **e**, Modification of the indicated HOIL-1L
580 proteins in *in vitro* ubiquitination assays with Petit-SHARPIN C885A and HOIL-1L WT
581 or the indicated mutants, as assessed by immunoblotting.
582 The data shown were repeated three times, independently, with similar results.
583 Unprocessed immunoblots are provided in Unprocessed Blots Figure 4.
584
585 **Fig.5 | HOIL-1L ubiquitinates all LUBAC subunits, followed by HOIP-mediated**
586 **linear ubiquitination onto mono-ubiquitin, and OTULIN counteracts this effect.**
587 **a–e** Modification of LUBAC subunits in WT or OTULIN KO MEFs expressing the
588 indicated HOIL-1L proteins. **a,d,** The indicated proteins in the lysates were probed as
589 indicated. **b,e**, Linear ubiquitin-specific tandem ubiquitin binding entity (M1-TUBE).
590 Material pulled down from the indicated MEFs with M1-TUBE were probed as indicated.
591 **c,** Modification of all LUBAC components in the presence of the indicated HOIL-1L and
592 Petit-SHARPIN C885A proteins in *in vitro* ubiquitination assays, as assessed by
593 immunoblotting with the indicated antibodies. **f**, Introduction of ligase-defective HOIL-
594 1L C458A together with HOIP and SHARPIN restored the OTULIN KO phenotype
595 induced by treatment with TNF-α (1 ng ml^{-1}) plus CHX (20 μg ml^{-1}). **g**, Viability of WT
596 or OTULIN KO MEFs expressing the indicated HOIL-1L proteins, stimulated with TNF-
597 α (10 ng ml^{-1}), was assessed using the iCELLigence system. **h**, Schematic of the
598 mechanism underlying HOIL-1L E3–mediated suppression of LUBAC activity. HOIL-
599 1L mono-ubiquitinates all LUBAC subunits (SHARPIN, HOIL1 and HOIP), and HOIP

600 further conjugates linear ubiquitin chains to mono-ubiquitin, which is conjugated to
601 LUBAC by HOIL-1L, as cis-linear ubiquitination (second, left). HOIL-1L E3 renders
602 HOIP RBR able to preferentially recognize LUBAC over other substrates including
603 NEMO or RIPK1 for linear chain conjugation as trans-linear ubiquitination, thereby
604 suppressing LUBAC functions. OTULIN counteracts cis-linear ubiquitination of
605 LUBAC, as reported previously. Loss of mono-ubiquitination of LUBAC following
606 deletion of HOIL-1L E3 profoundly suppresses cis-linear ubiquitination of LUBAC and
607 increases its linear ubiquitination activity towards substrates (trans-linear ubiquitination).
608 The data shown were repeated three times, independently, with similar results.
609 Unprocessed immunoblots are provided in Unprocessed Blots Figure 5.
610
611 **Fig. 6 | Defective HOIL-1L E3 activity protects against *Salmonella typhimurium***
612 ***infections* by activating LUBAC.**
613 **a–e,** *S. typhimurium* infections of LUBAC TKO MEFS stably expressing HOIP,
614 SHARPIN, and 3×FLAG–HOIL-1L WT or C458A. Quantification of intracellular *S.*
615 *typhimurium* proliferation, presented as mean colony forming units (CFUs) per well.
616 Mean ± S.D. is shown; n=3 independent experiments; *P*-values are from one-way
617 ANOVA followed by Tukey's multiple comparison test (**a**). Microscopic images of the
618 indicated MEFs infected with *S. typhimurium*. Scale bars, 100 μm. The experiments were
619 repeated three times, independently, with similar results. (**b**). Cell death induced by *S.*
620 *typhimurium* was monitored by assaying for LDH activity. Mean ± S.D. is shown; n=3
621 independent experiments; *P*-values from one-way ANOVA followed by Tukey's multiple

622 comparison test are shown (**c**). **d**, Structured illumination micrographs. The indicated
623 MEFs were infected with *S. typhimurium* and stained for linear ubiquitin, 3×FLAG–
624 HOIL-1L, or Hoechst 33342 at 6 h post-infection. Scale bars, 2 μm. The experiments
625 were repeated three times, independently, with similar results. **e**, qPCR analyses of
626 expression levels of the NF-κB target genes *Il6* and *Tnf* in cells infected with *S.*
627 *typhimurium* at 4 h post-infection. Mean is shown; n=3 independent experiments; *P*-
628 values are from one-way ANOVA followed by Tukey's multiple comparison test.
629 Statistical source data are provided in Statistical Source Data Fig. 6.
630
631 **Fig. 7 | Generation of HOIL-1L E3–defective ΔRING1 mice.**
632 **a,** Macroscopic pictures of the indicated littermate mice at 18 weeks old (left panel) and
633 12 months old (right panel). **b,** Lysates from organs of 9-week-old littermate mice of the
634 indicated genotypes were subjected to immunoblotting for linear ubiquitin. **c,**
635 Immunostaining for linear ubiquitin in 12-week-old littermate mice. Linear ubiquitin,
636 green; DAPI, blue. Scale bars, 50 μm. **d,** Macroscopic appearance of spleens of the
637 indicated mice at 18 weeks old. Scale bars, 1 cm. **e**, Histological analysis, performed by
638 H&E staining, of tissue sections from 9-week-old mice of the indicated genotypes. The
639 data shown in a-e were repeated twice, independently, with similar results. **f,** Antibody
640 titers of serum of the indicated mice were determined by ELISA. Mean ± S.D. is shown;
641 n=5 independent experiments; *P*-values were obtained by a two-tailed Student's t-test.
642 n.s. means not significant. **g,h,** Splenocytes of littermate mice of the indicated genotypes
643 at 15 weeks old were examined by flow cytometry. $CD19^+$ B cells of splenocytes were

analyzed for surface expression of CD38 and PNA (**g**, upper panel), FAS and PNA (g, lower panel), and TCRβ+CD4+ T cells of splenocytes were analyzed for surface expression of CD25 (**h**), all hallmarks of activated lymphocytes, are indicated. Figures exemplifying the gating strategy for flow cytometry experiments were provided in Supplementary Figure 1a,b. The data shown in a,b, d,e, g,h were repeated three times, independently, with similar results and the data shown in c were repeated twice, independently, with similar results.

Statistical source data are provided in Statistical Source Data Fig. 7 and unprocessed immunoblots are provided in Unprocessed Blots Figure 7.

Fig. 8 | Pathophysiological roles of HOIL-1L E3–defective mice.

a, Hepatocyte apoptosis induced by D-GalN (700 mg per kg) and LPS (10 μg per kg) in mouse livers of the indicated genotypes. Acquisition of macroscopic images, H&E staining, immunostaining for cleaved caspase-3 and TUNEL staining in livers of the indicated genotypes were performed 7 h after i.p. injections. The experiments were repeated twice, independently, with similar results. **b,** Kaplan–Meier survival graph comparing the two strains of mice up to 24 h after i.p. injections of LPS/D-Gal-N. *P*-values were obtained by a two-tailed log–rank test. **c**, Acquisition of macroscopic pictures, H&E staining, and immunostaining for cleaved caspase-3 and cleaved caspase-8 were performed in skin sections from 10-week-old mice of the indicated genotypes. The experiments were repeated three times independently, with similar results. **d, e,** Severity scores of dermatitis in mice of the indicated genotypes from 3 weeks to 10 weeks.

666 SHARPIN$^{cpdm/cpdm}$HOIL-1L$^{+/+}$ (n=14), SHARPIN$^{cpdm/cpdm}$HOIL-1L$^{\Delta RING1/+}$ (n =20),
667 SHARPIN$^{cpdm/cpdm}$HOIL-1L$^{\Delta RING1/\Delta RING1}$ (n =13). Data are means ± S.D.; *P*-values are
668 from one-way ANOVA followed by Tukey's multiple comparison test. Statistical
669 source data are provided in Statistical Source Data Fig. 8.

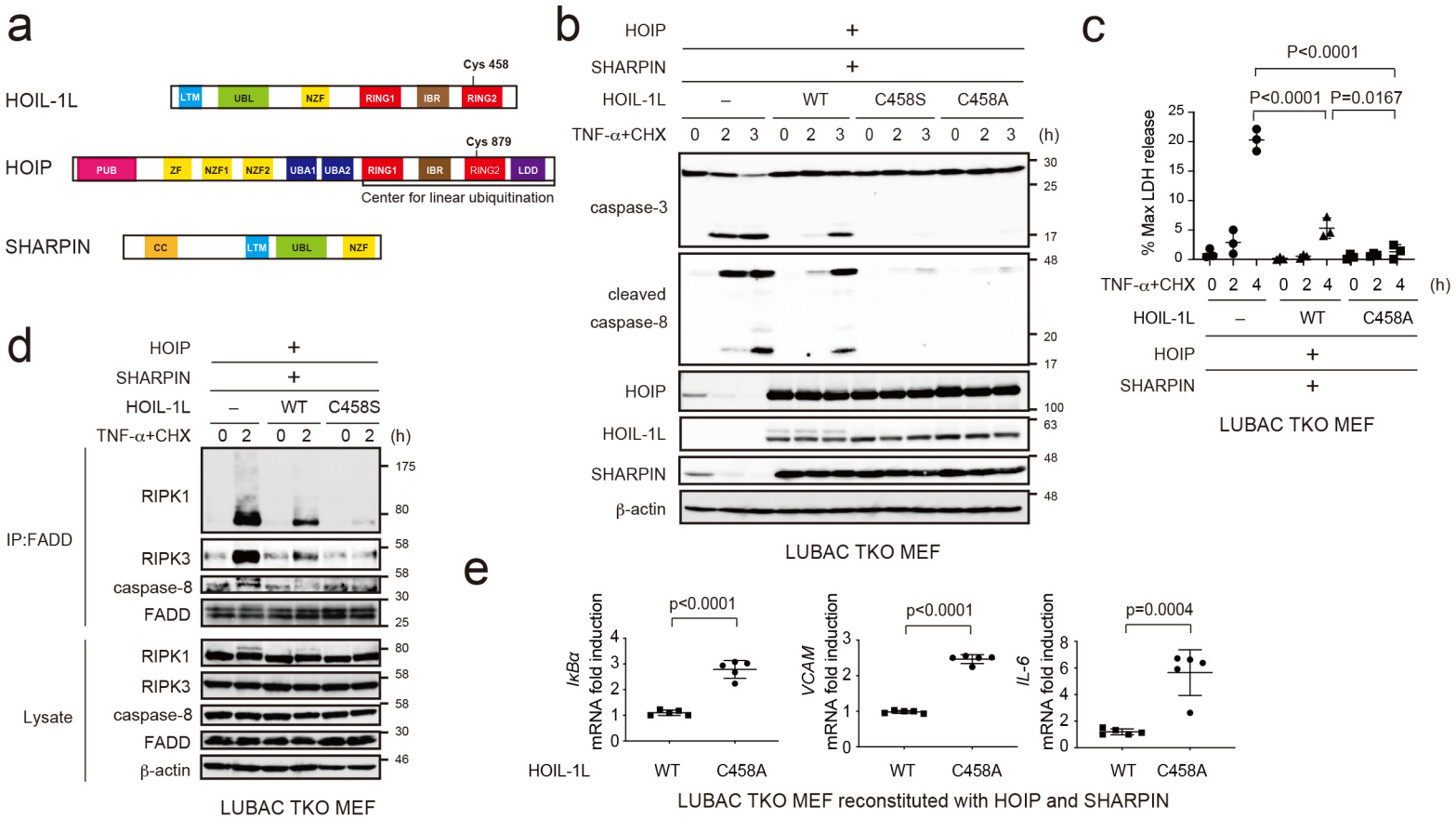

Fuseya et al. Figure1

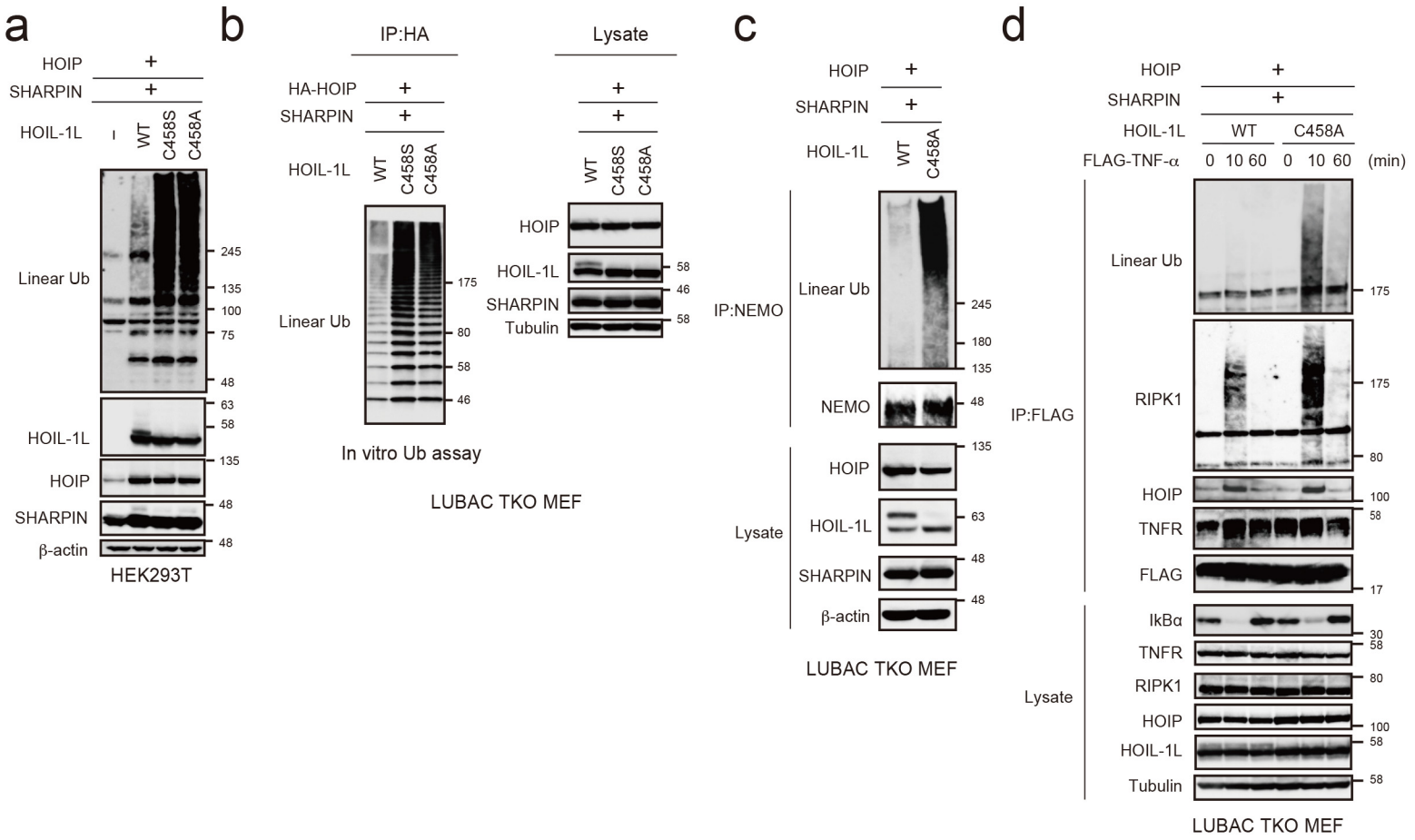

Fuseya et al. Figure2

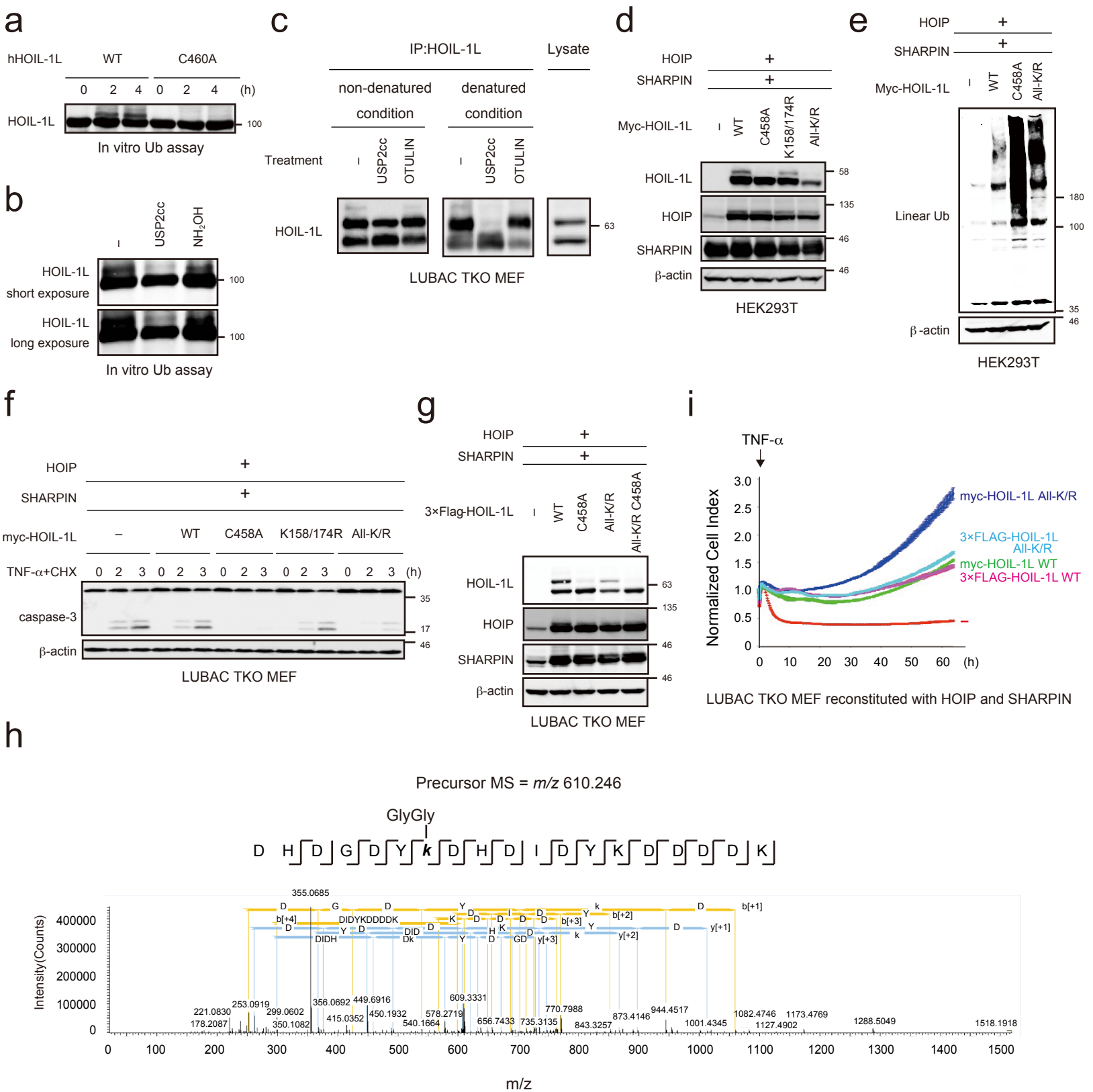

Fuseya.et.al. Figure3

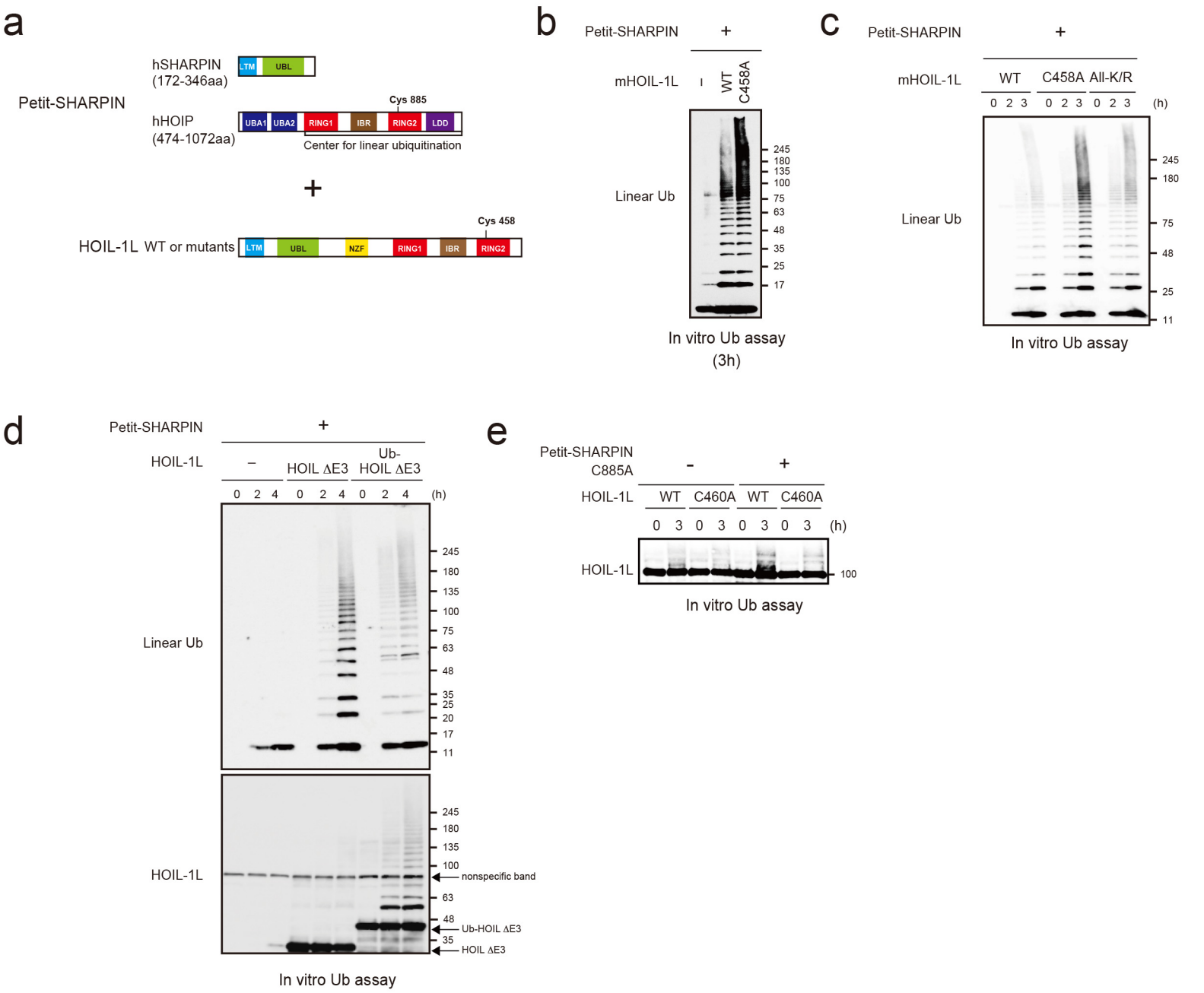

Fuseya et al. Figure4

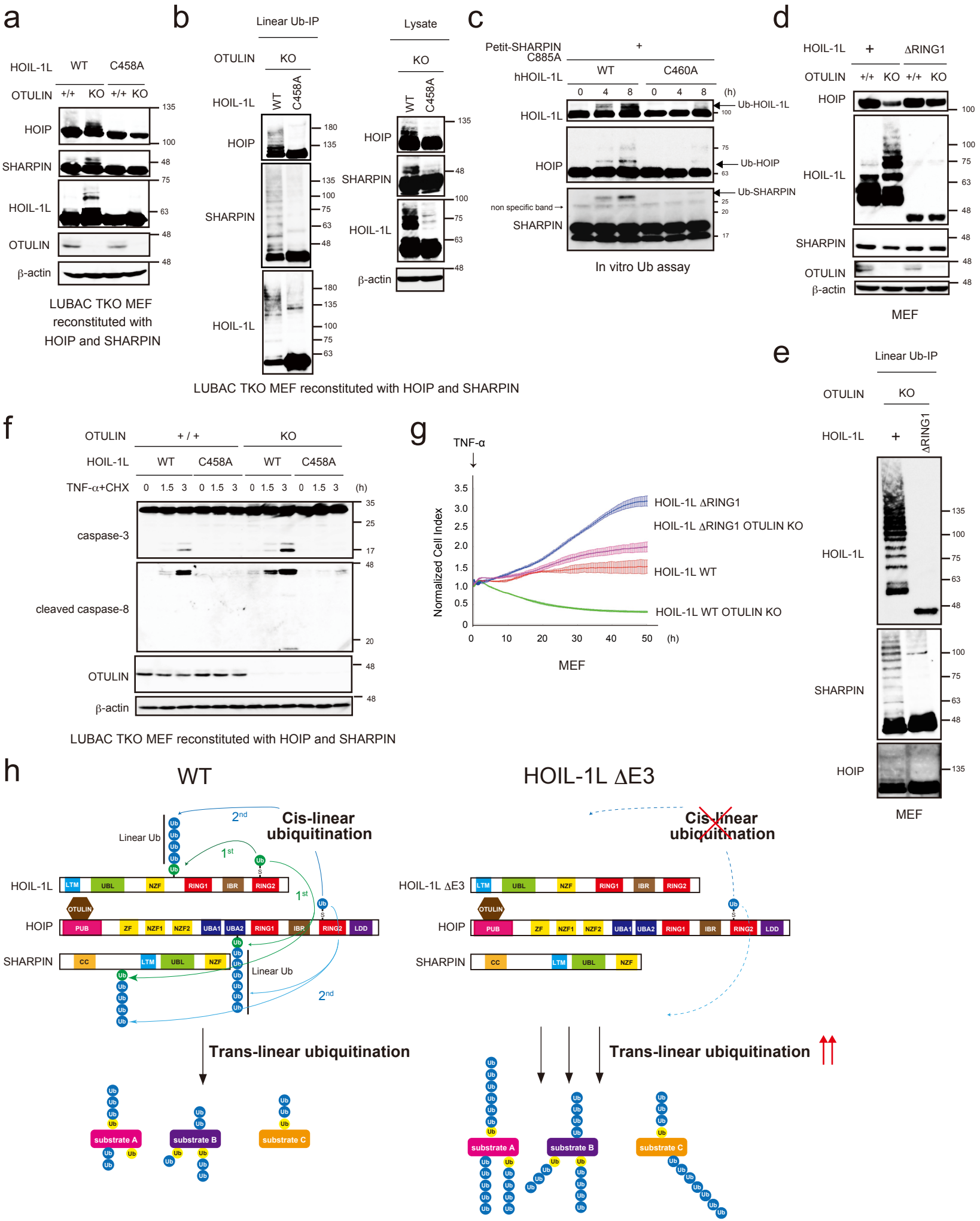

Fuseya et al. Figure 5

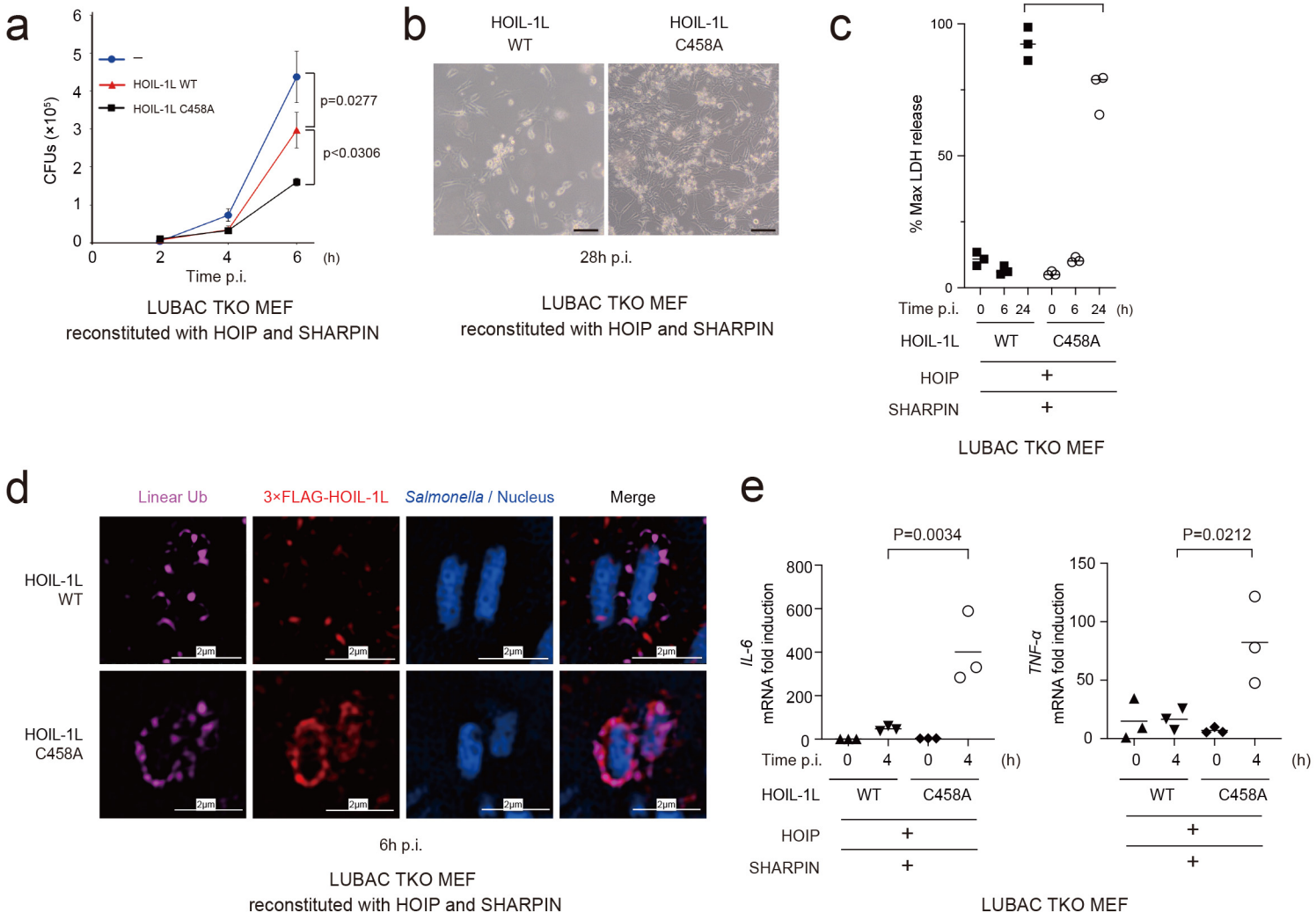

Fuseya et al. Figure 6

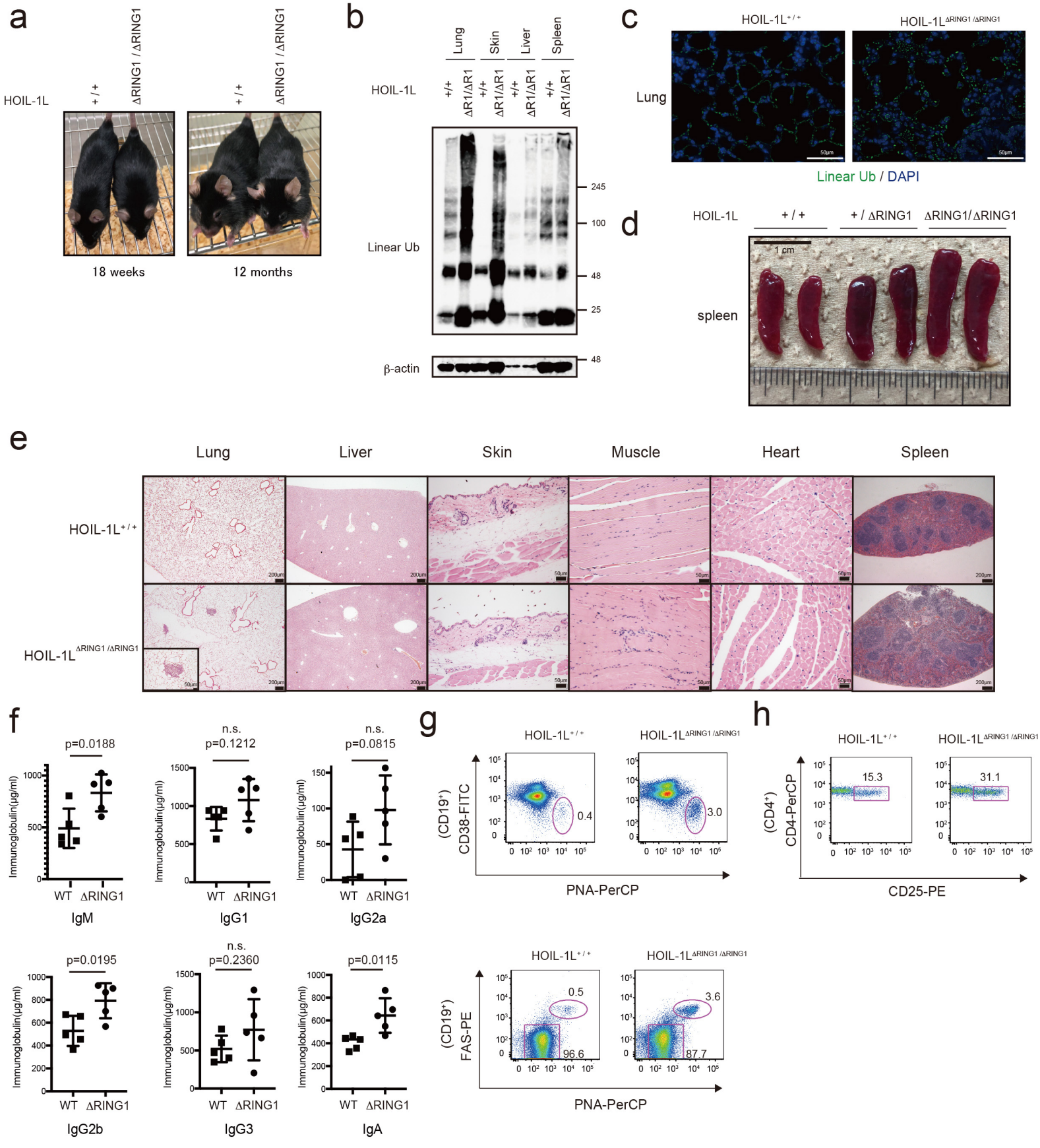

Fuseya et al. Figure 7

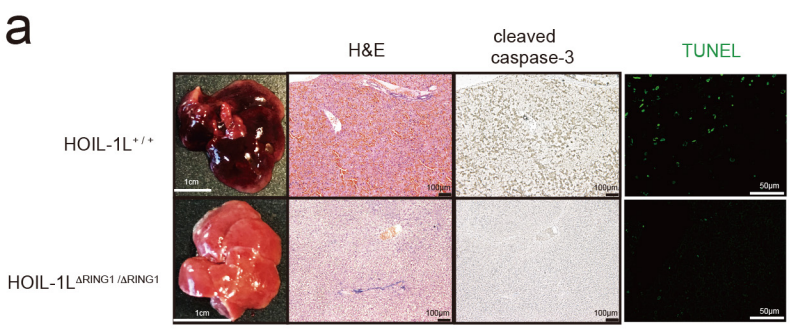

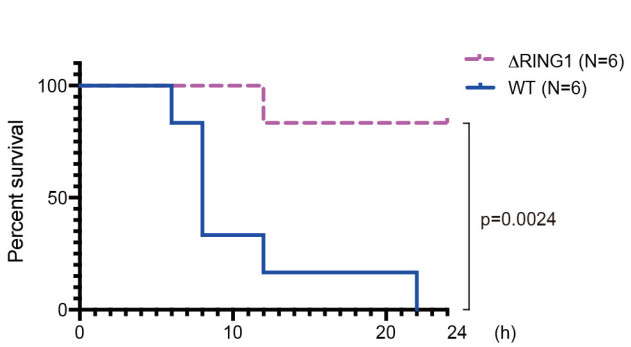

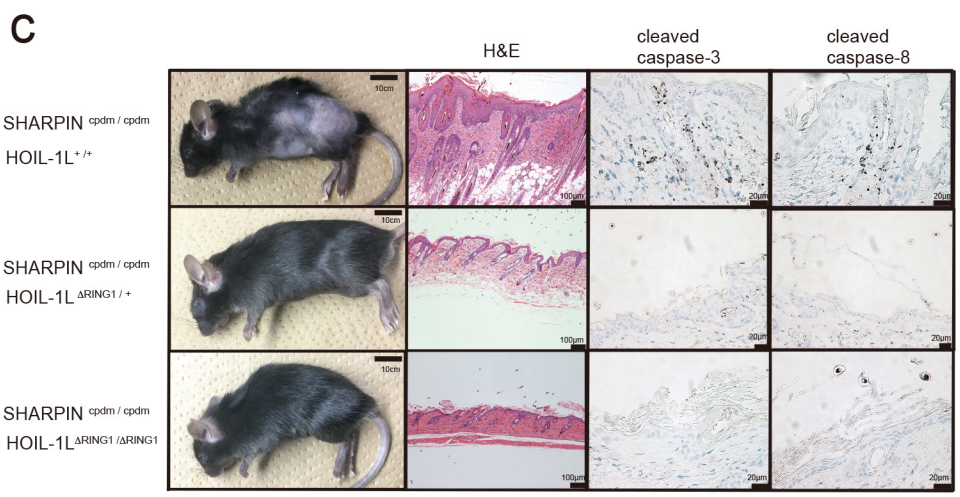

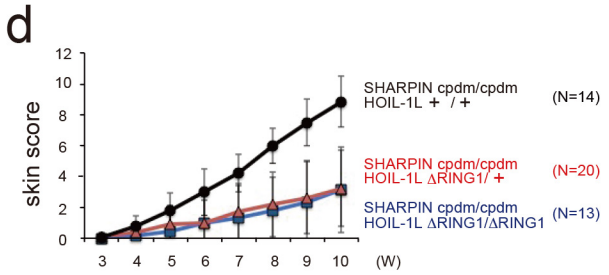

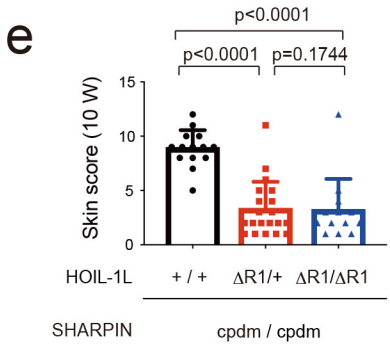

Fuseya et al. Figure 8

Methods

Cell cultures, transfection, and retroviral expression

MEFs and HEK293T cells were grown in DMEM containing 10% FBS, 100 IU ml^{-1} penicillin, and 100 μg ml^{-1} streptomycin. Keratinocytes were cultured in serum-free human keratinocyte medium (DS Pharma Biomedical) supplemented with bovine pituitary extract. Primary hepatocytes were grown in William's E medium (Gibco) supplemented with 10% FBS, GlutaMAX (Gibco/Thermo Fisher Scientific), penicillin, streptomycin, 2 μg ml^{-1} insulin, and 100 nM dexamethasone. Transfections were performed using Lipofectamine 2000 (Invitrogen). For retroviral expression, pMXs-IP, pMXs-neo, or pMXs-IRES-Bsr encoding LUBAC components was transfected into Plat-E packaging cells as described previously[16]. The resultant viruses were used to infect LUBAC TKO cells, and stably transduced cells were selected using puromycin, G-418, or blasticidin.

Plasmids, antibodies, and reagents

cDNAs used in this study were described previously[16,29,37]. Two deletion mutants were generated from the amplified ORF of mouse HOIL-1L: before RING1 (aa 1–279) and before NZF (aa 1–189). Mutants of mHOIP (C879A) and mHOIL-1L (C458A, C458S) were generated by two-step PCR. cDNAs were ligated into the appropriate epitope-tag sequences and then cloned into pcDNA3.1, pMAL-c2x, pT7-7, pMXs-IP, pMXs-neo, pMXs-IRES-Bsr, or pSpCas9(BB)-2A-Puro (PX459) (#48139, Addgene)[58]. A synthetic cDNA encoding HOIL-1L All-K/R was purchased from Eurofins. Antibodies are listed in

Supplementary Table 1.

qRT-PCR

For real-time quantitative reverse transcription PCR (qRT-PCR), total RNA was isolated using the RNeasy Mini Kit (Qiagen). DNase-treated RNA (100 ng) was reverse-transcribed to cDNA using the High Capacity RNA-to-cDNA Kit (Thermo Fisher Scientific). Real-time PCR was performed with Power SYBR Green PCR Master Mix (Applied Biosystems) in an ABI ViiA7 Real-Time PCR system (Applied Biosystems). Primers are listed in Supplementary Table 2. All gene expression levels were normalized against the corresponding levels of *Actb* (encoding β-actin).

Immunoprecipitation, immunoblotting, and deubiquitination analysis

Cells were lysed with lysis buffer containing 50 mM Tris-HCl (pH 7.5), 150 mM NaCl, 1% Triton X-100, 2 mM phenylmethylsulfonyl fluoride (PMSF), and protease inhibitor cocktail (Sigma-Aldrich) with or without 10 mM N-ethylmaleimide (NEM). Lysates were clarified by centrifugation at 15,000 rpm for 20 min at 4°C. For lysates of mouse tissues, 50 mg samples of tissue were homogenized and lysed with the lysis buffer described above. For denaturing conditions, cells were lysed in phosphate-buffered saline (PBS) containing 1% SDS and then heated at 95°C for 10 min to disrupt noncovalent interactions. After heating, lysates were sheared with a 25-gauge needle and

centrifuged at 15,000 rpm for 5 min at room temperature; the resultant supernatant was diluted to 0.1% SDS with lysis buffer mentioned above. For immunoprecipitations, Protein G beads (Thermo Fisher Scientific) were prepared by washing three times with PBS and then incubated with the appropriate antibodies for 1 h at 4°C. The antibody-bead conjugates were then incubated with lysates for 2 h at 4°C, followed by five washes with lysis buffer. For deubiquitination analysis, USP2cc (5 μg) or OTULIN (5 μg) in 20 μl buffer containing 20 mM Tris-HCl (pH 7.5) and 5 mM DTT was added to immunoprecipitated beads or 30 μg cell lysate, and then incubated at 37°C for 60 min.

Immunoprecipitation of TNFR Complex I

After treatment with FLAG-His-TNF-α (1 μg ml^{-1}), cells were lysed with lysis buffer containing 10 mM Tris-HCl (pH 7.5), 150 mM NaCl, 0.2% NP-40, 10% glycerol, 2 mM PMSF, and protease inhibitor cocktail; centrifuged at 10,000 *g* for 20 min at 4°C; and immunoprecipitated with anti-FLAG M2 antibody. Immunoprecipitated TNFR1 complex was eluted by incubation at 37°C for 40 min in 30 μl TBS buffer containing 400 ng μl^{-1} of 3×FLAG peptide (Sigma-Aldrich), and then analyzed by immunoblotting.

Immunoprecipitation of TNFR Complex II

Cells were pretreated with Z-VAD-FMK (10 μM) (MBL) for 60 min, and then

67 stimulated with TNF-α (2.5 ng ml-1) and CHX (20 μg ml-1) for the indicated
68 periods. Cells were lysed with lysis buffer containing 30 mM Tris-HCl (pH
69 7.5), 120 mM NaCl, 1% Triton X-100, 10% glycerol, 2 mM PMSF, and protease
70 inhibitor cocktail, followed by centrifugation at 10,000 *g* for 10 min at 4°C.
71 The cleared lysates were immunoprecipitated with anti-FADD antibody.
72
73 **Luciferase assays**
74 HEK293T cells were transfected with pGL4.32 (Luc2p/NF-κB–RE/Hygro) and
75 pGL4.74 (hRLuc/TK) (Promega) along with plasmids encoding WT or mutant
76 LUBAC components. Twenty-four hours after transfection, cells were lysed,
77 and luciferase activity was measured using the Dual-Luciferase reporter
78 assay system (Promega) on a Lumat Luminometer (Berthold).
79
80 **Cell viability assay using real-time cellular analysis (RTCA) technology**
81 Cell viability was continuously monitored as an impedance-based cell index
82 using the iCELLigence system (ACEA Bioscience). For each sample, 20,000
83 cells were plated onto an E-Plate L8. The next day, cells were treated with
84 TNF-α (10 ng ml-1), and the cell index was continuously monitored. Data were
85 normalized against cell indices at the time of TNF-α treatment.
86
87 **Measurement of lactate dehydrogenase (LDH) release**
88 LDH release was measured using the Cytotox96 Non-Radioactive

Cytotoxicity Assay kit (Promega). Briefly, cells were seeded on a 24-well plates at 1×10^5 or 2×10^4 cells per well, and then treated with TNF-α (10 ng ml^{-1}) plus CHX (20 μg ml^{-1}) or *S. typhimurium*, respectively. After culture for the indicated periods, the media were collected. LDH level in culture media was determined by measuring absorbance at 490 nm on a SpectraMax M5 (Molecular Devices).

In vitro ubiquitination assay

Anti-HA immunoprecipitates from cells expressing HA-HOIP, Petit-SHARPIN, or Petit-SHARPIN C885A along with recombinant HOIL-1L (WT or mutant) were incubated at 37°C for the indicated periods with E1 (100 ng), UbcH7/UBE2L3 (400 ng), ubiquitin (5 μg), and 2 mM ATP in 20 μl buffer containing 20 mM Tris Tris-HCl (pH 7.5), 5 mM $MgCl_2$, and 1 mM DTT. For deubiquitination analysis of HOIL-1L, recombinant HOIL-1L WT or mutants were incubated overnight at 37°C with E1 (100 ng), UbcH7/UBE2L3 (400 ng), ubiquitin (5 μg), and 2 mM ATP in 20 μl buffer containing 20 mM Tris-HCl (pH 7.5), 5 mM $MgCl_2$, and 1 mM DTT. After the overnight incubation, NH_2OH (0.5–1.5 M) or USP2cc (5 μg) was added, and the sample was incubated at 37°C for 60 min. After incubation, reactions were terminated by addition of SDS sample buffer and analyzed by SDS-PAGE followed by immunoblotting.

Expression and purification of recombinant proteins

MBP-mHOIL-1L (WT, C458A, and All-K/R), MBP-hHOIL-1L (WT, C460A), hHOIL-1L ΔE3-Strep, [aa 1–281], Ub-hHOIL-1L ΔE3-Strep, MBP-hOTULIN, His_6-USP2cc, and Petit-SHARPIN C885A were expressed in *E. coli* BL21 cells (CodonPlus DE3 #230280). MBP-fusion, Strep-tagged, and His_6-tagged proteins were purified using amylose resin (New England BioLabs), Strep-Tactin XT Superflow High Capacity (IBA Lifesciences), and Ni-NTA Agarose (QIAGEN), respectively. Petit-SHARPIN, recombinant E1, and recombinant UbcH7/UBE2L3 were prepared and purified as described previously[8,37,23].

Mass spectrometric analysis

LUBAC TKO MEFs stably reconstituted with human SHARPIN, myc-human HOIP, and 3×FLAG-human HOIL-1L WT or C460A were subjected to MS. HOIL-1L was immunoprecipitated with anti-DDDDK (FLA-1), followed by separation with SDS-PAGE and staining with Bio-Safe Coomassie (Bio-Rad). Gel regions corresponding to molecular weights of interest were excised. For reduction and alkylation of cysteine residues (Fig. 3h and S3e), the gels were incubated for 1 h with 5 mM TCEP and subsequently for 10 min with 5 mM methyl methanethiosulfonate (MMTS) in 50 mM ammonium bicarbonate (AMBC). The gel pieces were washed in 50 mM AMBC/30% acetonitrile (ACN) for 2 h, and then with 50 mM AMBC/50% ACN for 1 h. The gel pieces were then dehydrated in 100% ACN for 15 min. Proteins were digested with 20 ng

μl-1 sequence grade trypsin (Promega) in 50 mM AMBC/5% ACN, pH 8.0, at 37°C for 16 h. The digested peptides were extracted four times with 0.1% trifluoroacetic acid (TFA)/70% ACN. Peptides were concentrated by vacuum centrifugation and resuspended in 0.1% TFA.

For MS analysis, an Easy nLC 1200 (Thermo Fisher Scientific) was connected online to an Orbitrap Fusion LUMOS (Thermo Fisher Scientific) with a nanoelectrospray ion source (Thermo Fisher Scientific). Peptides were loaded onto a C18 analytical column (IonOpticks, Aurora Series Emitter Column, AUR2-25075C18A 25 cm × 75 μm 1.6 μm FSC C18 with nanoZero fitting) and separated using an 80 or 90 min gradient (solvent A, 0.1% FA; solvent B, 80% ACN/0.1% FA). For parallel reaction monitoring, the Orbitrap Fusion LUMOS instrument was operated in targeted MS/MS mode by the Xcalibur software (Thermo Fisher Scientific), and the peptides were fragmented by higher-energy collisional dissociation (HCD) with a normalized collision energy of 30. MS/MS resolution, target AGC values, and isolation windows were set to 30,000, 5E4, and 2.0 *m/z*, respectively. For data-dependent acquisition of MS/MS spectra, the most intense ions (Cycle Time: 1 sec) with charge states from +2 to +7 were selected for fragmentation by HCD with a normalized collision energy of 30, and fragment ions were detected using an Ion Trap. AGC target and isolation window were set to 1E4 and 1.6 *m/z*, respectively. Easy nLC 1000 (Thermo Fisher Scientific) and Q Exactive (Thermo Fisher Scientific) instruments were used for acquisition of the data shown in Fig. S3e, for which peptides were separated on C18 analytical columns (Reprosil-Pur 3 μm, 75 μm i.d. × 12 cm packed

154 tip column, Nikyo Technos Co., Ltd) with a 90 min gradient (solvent A, 0.1% FA; solvent
155 B, 100% ACN/0.1% FA). The Q Exactive instrument was operated in data-dependent
156 mode using the Xcalibur software, and the top 10 most intense ions with charge states
157 from +2 to +4 were selected for fragmentation by HCD with a normalized collision
158 energy of 28. The data were analyzed using SEQUEST in Proteome Discoverer 2.2
159 (Thermo Fisher Scientific). The mass tolerances for the precursor and fragment ions were
160 10 ppm and 20 mmu (for Orbitrap) or 0.6 Da (for Ion Trap), respectively, and peptide
161 identification was filtered at FDR < 0.01.

162 Absolute quantification (AQUA) of ubiquitin linkages was performed
163 essentially as previously described[59] with some modifications. Whole-cell lysates (24 μg)
164 were separated by SDS-PAGE, and gel regions > 75 kD were excised for in-gel trypsin
165 digestion as described above. After trypsin digestion, AQUA peptides (15 fmol/injection)
166 were added to the extracted peptides. Concentrated peptides were diluted with 20 μL
167 0.1% TFA containing 0.05% H_2O_2 to oxidize methionine residues and then incubated at
168 4°C overnight. Easy nLC 1200 and Orbitrap Fusion LUMOS were operated as described
169 above, and peptides were separated using a 45 min gradient. The data were processed
170 using the PinPoint software 1.3 (Thermo Fisher Scientific), and peptide abundance was
171 calculated based on the integrated area under the curve of the selected fragment ions.

172 **Generation of knockout cells by CRISPR/Cas9**

173 Generation of LUBAC TKO MEFs was described previously[16]. To knock out OTULIN,
174 wild-type, ΔRING1, or TKO MEFs reconstituted with HOIP and SHARPIN were

transfected with pX459 encoding a gRNA sequence targeting OTULIN (ACTTCCATAAGGCGAGTCCG). Transfections were performed using Lipofectamine 2000, followed by selection with puromycin for 2 days. Isolated colonies were verified as OTULIN KO by immunoblotting with anti-OTULIN antibody and by genomic PCR using the following primers:

OTULIN typing_Fwd: 5'- TGGGGGTCCCATACTAGATA -3'

OTULIN typing_Rev: 5'- ACACTGCATGTAACACCTTC-3'

Tandem ubiquitin binding entity (TUBE) assay

Halo-tagged linear ubiquitin chain-specific tandem ubiquitin binding entity (M1-specific TUBE) was purified as described previously[60,61]. To measure linear ubiquitination in MEFs, 2 mg cell lysates were incubated at 4°C for 3 h with 2 μg M1-specific TUBE coupled with 20 μl of equilibrated Magne HaloTag beads (Promega) in buffer containing 50 mM Tris-HCl (pH 7.5), 150 mM NaCl, and 1% Triton X-100. The precipitates were washed five times with 0.005% Nonidet P40 Substitute in PBS, boiled in SDS sample buffer, and analyzed by immunoblotting.

***S. typhimurium* infection**

S. typhimurium (NBRC13245) was purchased from the National Institute of Technology and Evaluation, Biological Resource Center, Japan. Before each infection experiment, *S. typhimurium* strains were freshly streaked from glycerol stocks on Luria-Bertani (LB) plates supplemented with the appropriate antibiotics. The next day, a single colony was

197 inoculated into LB supplemented with antibiotics, grown overnight, and subcultured
198 (1:30) in fresh LB for 3 h at 37°C to reach an optical density at 600 nm (OD_{600}) of 1.
199 MEFs were maintained in DMEM without antibiotics. Infections were performed at a
200 multiplicity of infection (MOI) of 100 for 30 min at 37°C in pre-warmed DMEM lacking
201 antibiotics. Following three washes with warm PBS, medium was replaced with DMEM
202 supplemented with 100 μg ml^{-1} gentamycin (Sigma-Aldrich), and cells were maintained
203 for the indicated time periods at 37°C. To count intracellular bacteria, cells from
204 quadruplicate wells were lysed with 0.1% Triton X-100 (v/v) in sterile saline, and serial
205 dilutions were spread on LB plates and incubated at 37°C.
206
207 **Microscopy**
208 *S. typhimurium* or GFP-expressing *S. typhimurium*-infected cells were fixed in 4%
209 paraformaldehyde PBS (Fujifilm) for 15 min at 37°C. Cells were washed three times with
210 PBS, followed by permeabilization with 0.2% Triton X-100 in PBS for 10 min at room
211 temperature. Cells were subsequently blocked with 2% BSA in PBS for 30 min at room
212 temperature. Cells were incubated with the indicated primary antibodies for 16 h at 4°C.
213 Cells were washed three times with PBS and then incubated with the appropriate
214 secondary antibodies. After washing, nuclei and *S. typhimurium* were counterstained with
215 Hoechst 33342 (Invitrogen) and mounted in VECTASHIELD antifade reagent (Vector
216 Laboratories) on microscopic glass supports. Confocal images were obtained on a Zeiss
217 710 confocal microscope (ZEISS). SIM images were obtained using a Nikon N-SIM
218 system equipped with a 100×/1.49 TIRF oil immersion objective lens (Nikon). Image

processing, including three-dimensional reconstruction and co-localization analysis, were carried out using the NIS-Element advanced research software (Nikon).

Mice and preparation of primary cells

SHARPIN$^{cpdm/cpdm}$ mice were obtained from the Jackson Laboratory. To generate KO mice harboring a conditional deletion of exons 7 and 8 of the gene encoding HOIL-1L (HOIL-1L ΔRING1 cKO), the targeting vector shown in Extended Data Fig. 7e was transfected into ES cells (TT2), and G418-resistant colonies were selected. Homologous recombinants were microinjected into 8-cell embryos of ICR mice. The resultant chimeric mice were intercrossed with C57BL/6 mice. Mice lacking HOIL-1L RING1 throughout the body (HOIL-1L ΔRING1) were generated by mating HOIL-1L ΔRING1 cKO with CAG-Cre mice (RBRC No. RBRC01828)[62]. Preparation of primary keratinocytes, hepatocytes, and MEFs were described previously[16,37,63]. All mouse protocols were approved by Kyoto University.

Acute liver injury model

Mice intraperitoneally injected with D-GalN (700 mg kg^{-1}) and LPS (10 μg kg^{-1}) or with PBS were euthanized at 7 h after treatment, and liver and serum samples were collected. For DNA extraction, 50 mg liver was lysed for 2 h at 55°C with lysis buffer containing 100 mM Tris-HCl (pH 8.5), 5 mM EDTA, 0.2% SDS, 40 mM NaCl, and proteinase K (0.1 mg ml^{-1}), followed by centrifugation at 13,000 rpm for 10 min. Genomic DNA was precipitated with isopropanol, and dried pellets were dissolved in TE buffer.

241

242 **Histology, TUNEL assay, and immunohistochemistry**

243 Samples were fixed in 4% buffered paraformaldehyde, followed by paraffin embedding.
244 Sections were subjected to TUNEL staining using the In Situ Cell Death Detection Kit,
245 Fluorescein (Roche Life Science). For immunohistochemistry, after antigen retrieval for
246 10 min at 99°C in citric buffer (pH 6), slides were blocked for 30 min with PBS containing
247 2% BSA, 5% goat serum, and 0.1% Triton X-100; incubated with primary antibody for
248 16 h at 4°C; and incubated for 1 h at room temperature with the appropriate Alexa Fluor
249 488-conjugated secondary antibody at a 1:200 dilution. After washing, the samples were
250 mounted with a coverslip using ProLong gold antifade reagent with DAPI (Thermo Fisher
251 Scientific) and imaged on a BZ-900 fluorescence microscope (Keyence) or FV1000D
252 confocal laser scanning fluorescence microscope (Olympus). For peroxidase staining,
253 slides were treated with 3% H_2O_2 for 10 min at room temperature, washed, blocked, and
254 incubated with a primary antibody as mentioned above. After washing, the slides were
255 incubated for 20 min with Simple Stain Mouse MAX-PO (Nichirei Biosciences), washed,
256 incubated with DAB (3,39-diaminobenzidine tetrahydrochloride) (Pierce), and
257 immediately washed and counterstained with hematoxylin.

258

259 **ELISA**

260 To measure total immunoglobulins, anti-mouse IgM, IgA, IgG1, IgG2a, IgG2b, and IgG3
261 antibodies (SouthernBiotech; all at 1 μg ml^{-1}) were added to 96-well ELISA plates (Nunc
262 MaxiSorp) and incubated at 4°C overnight. The wells were then blocked with 1% BSA

263 in PBS at 37°C for 75 min. Appropriately diluted serum was incubated at room
264 temperature for 60 min, and then HRP-conjugated anti-mouse IgM, IgA, IgG1, IgG2a,
265 IgG2b, and IgG3 antibodies (SouthernBiotech) were added. BD OptEIA (BD
266 Biosciences) was used as the substrate, and absorbance at 450 nm was measured using a
267 microplate reader (Molecular Devices).
268
269
270 **Flow cytometry analysis**
271 Single-cell suspensions prepared from the spleen of 8- to 15-week-old mice of the
272 indicated genotype were stained with fluorochrome-conjugated antibodies. All samples
273 were acquired using a FACSCanto II (BD Biosciences), and the results were analyzed
274 using the FlowJo software (Tree Star).
275
276 **Evaluation of dermatitis severity**
277 Severity of dermatitis was scored as 0 (none), 1 (mild), 2 (moderate), or 3 (severe). Areas
278 evaluated were the face, chest, abdomen, rostral back, and caudal back. The skin score
279 was the sum of each score obtained.
280
281 **Statistical analysis and Reproducibility**
282 Statistical analyses were performed using GraphPad Prism 8 version 8.4.0 (GraphPad
283 Software). Statistical significance was determined using, a two-tailed Student's t-test,
284 one-way ANOVA followed by Tukey's multiple comparison test or a two-tailed log–rank

test. The exact sample sizes (n) used to calculate statistics are provided in the figure legends. P values are provided in the figure legends. No data points were excluded. *P*-values < 0.05 were considered statistically significant. All experiments were reproduced with similar results at least twice.

Data Availability

Source data for Figs.1-8, Extended Data Figs.1-5,7,8 have been provided as Statistical Source data or Unprocessed Blots. All other data supporting the findings of this study are available from the corresponding author on reasonable request.

Supplementary information is available in the online version of this paper.

REFERENCES

58. Ran, F.A. *et al.* Genome engineering using the CRISPR-Cas9 system. *Nat. Protoc.* **8**, 2281-2308 (2013).
59. Ohtake, F., Saeki, Y., Ishido, S., Kanno, J. & Tanaka, K. The K48-K63 Branched Ubiquitin Chain Regulates NF-κB Signaling. *Mol. Cell* **64**, 251-266 (2016).
60. Hjerpe, R. *et al.* Efficient protection and isolation of ubiquitylated proteins using tandem ubiquitin-binding entities. *EMBO Rep.* **10**, 1250-1258 (2009).
61. van Wijk, S.J., Fiskin, E. & Dikic, I. Selective monitoring of ubiquitin signals with genetically encoded ubiquitin chain-specific sensors. *Nat. Protoc.* **8**, 1449-1458 (2013).
62. Matsumura, H., Hasuwa, H., Inoue, N., Ikawa, M. & Okabe, M. Lineage-specific cell disruption in living mice by Cre-mediated expression of diphtheria toxin A chain. *Biochem. Biophys. Res. Commun.* **321**, 275-279 (2004).
63. Tamiya, H. *et al.* IFN-γ or IFN-α ameliorates chronic proliferative dermatitis by

311 inducing expression of linear ubiquitin chain assembly complex. *J. Immunol.* **192**,
312 3793-3804 (2014).
313

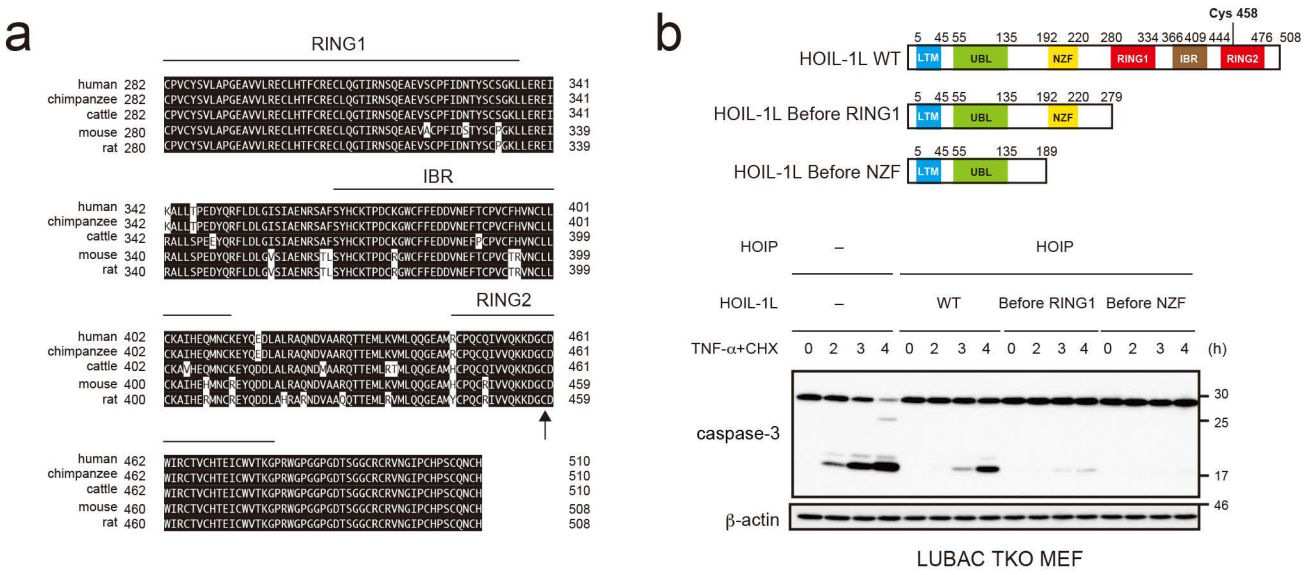

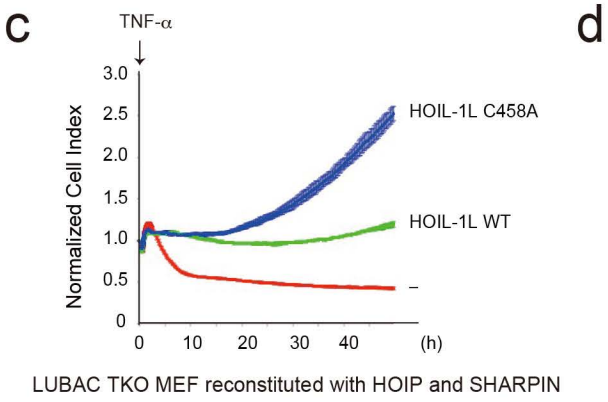

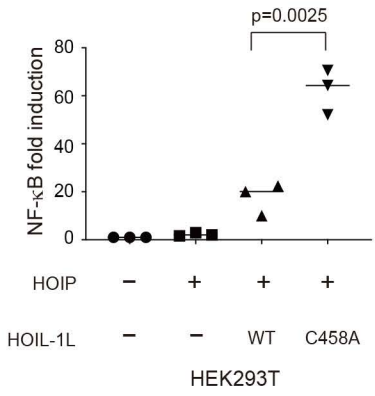

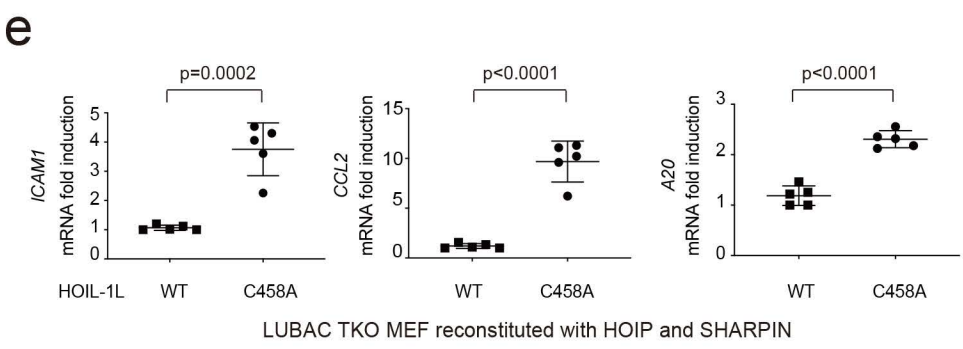

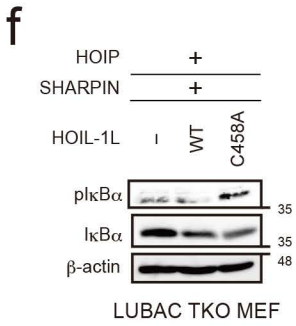

Fuseya et al. Extended Data Figure1

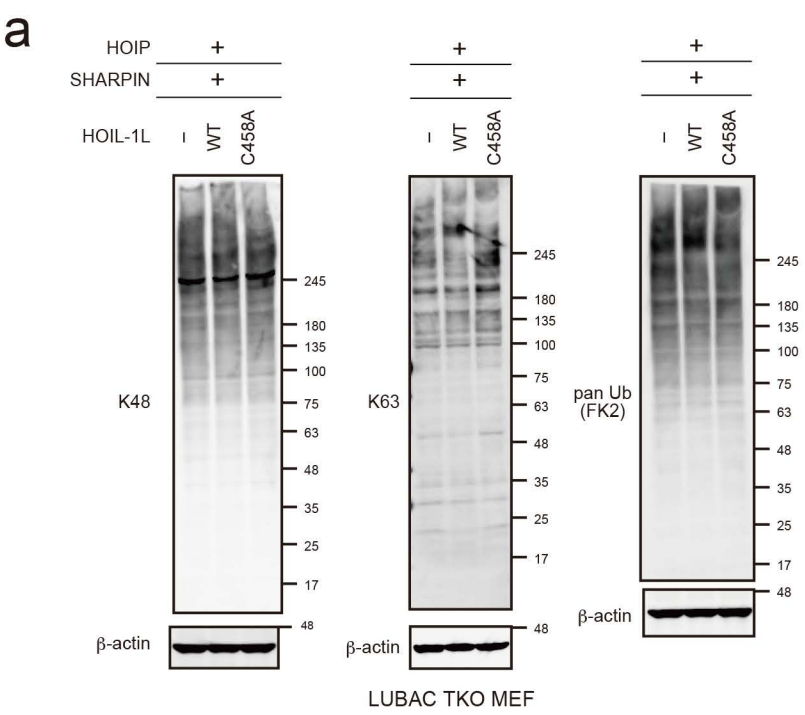

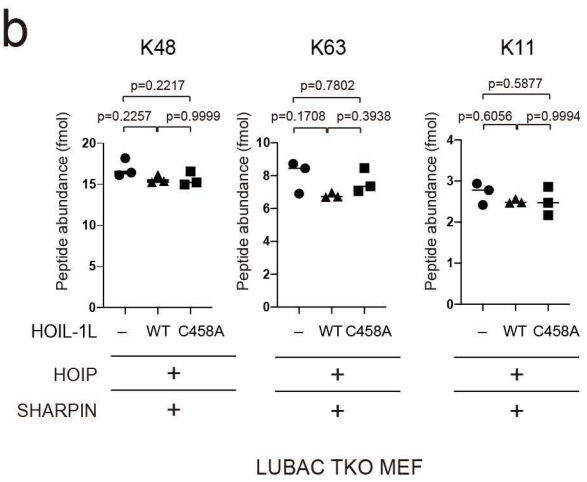

Fuseya et al. Extended Data Figure2

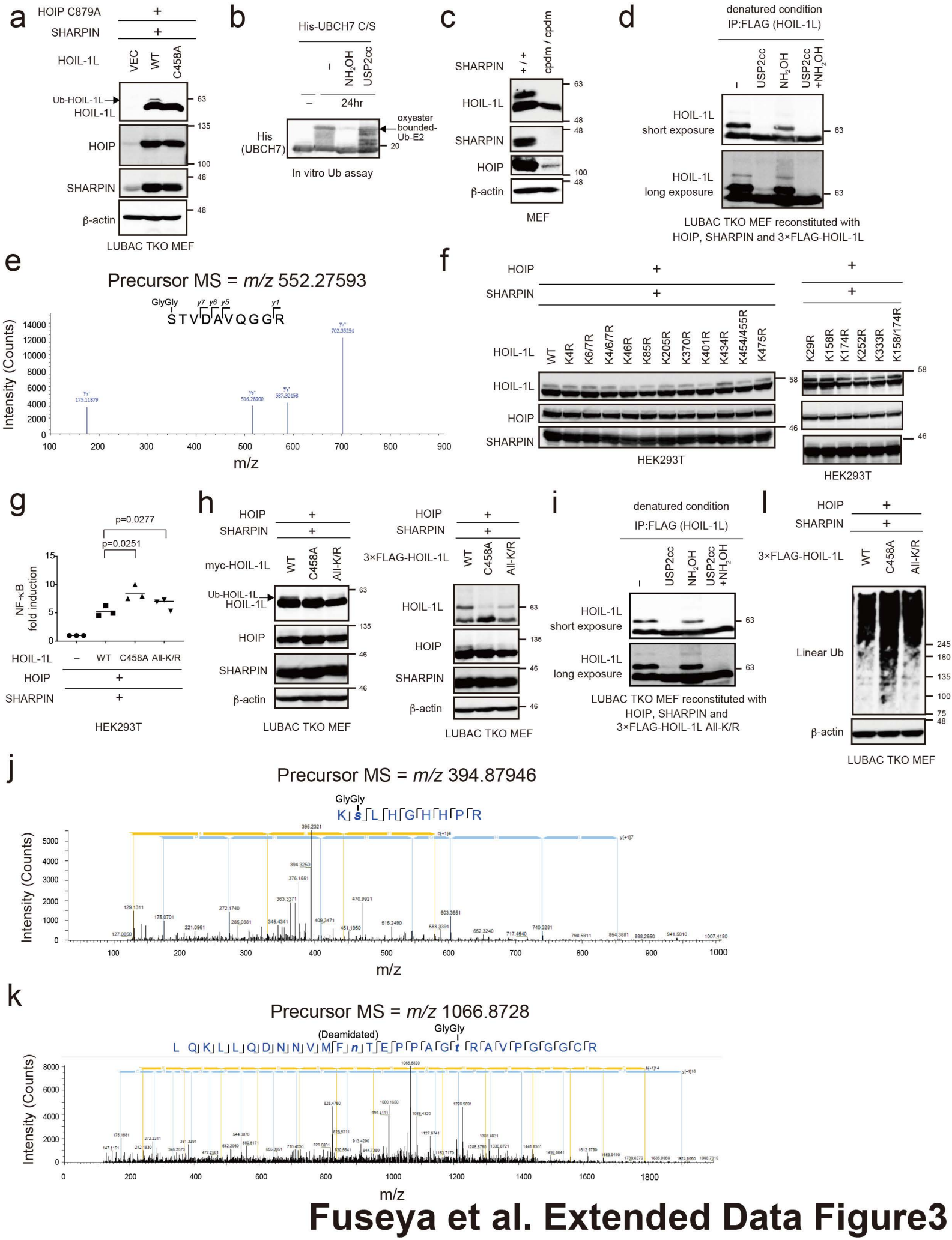

Fuseya et al. Extended Data Figure3

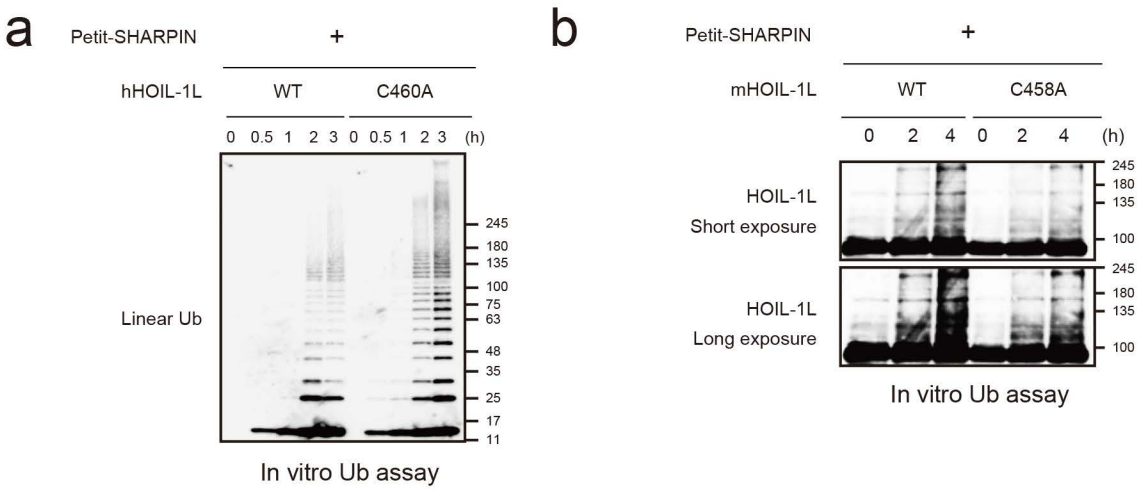

Fuseya et al. Extended Data Figure4

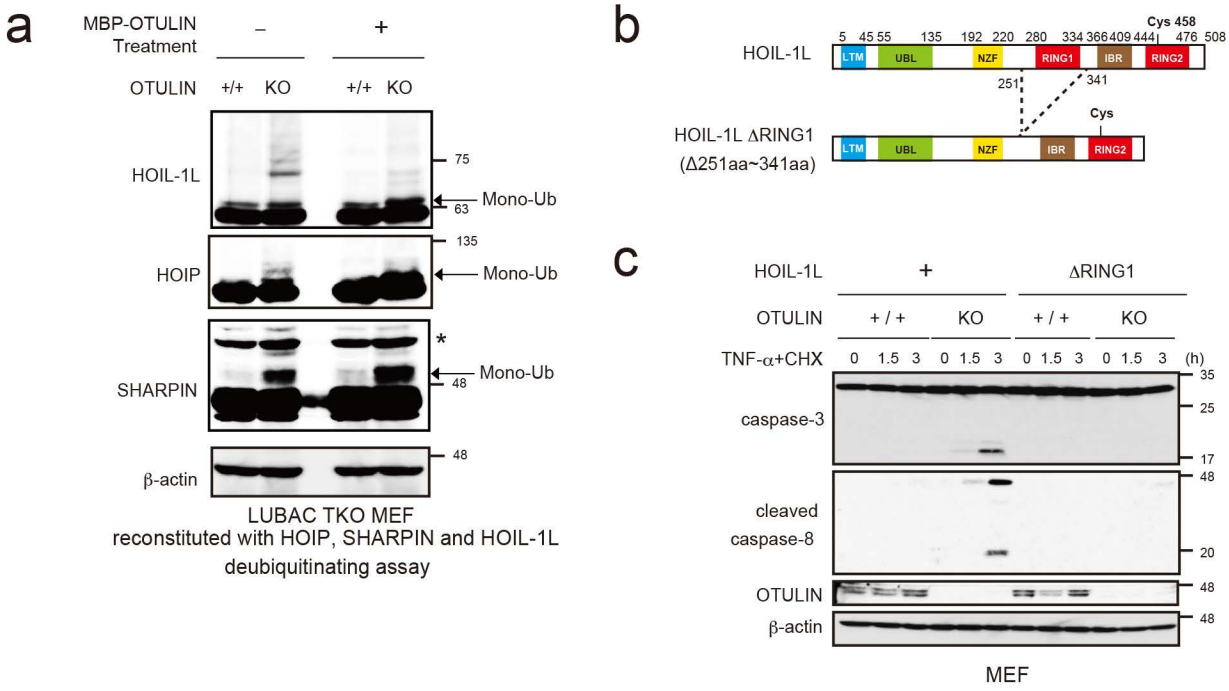

Fuseya et al. Extended Data Figure5

a

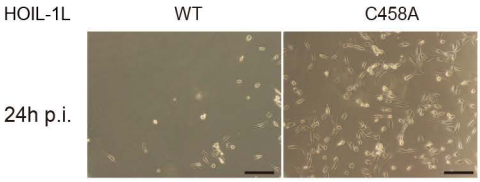

LUBAC TKO MEF reconstituted with HOIP and SHARPIN

b

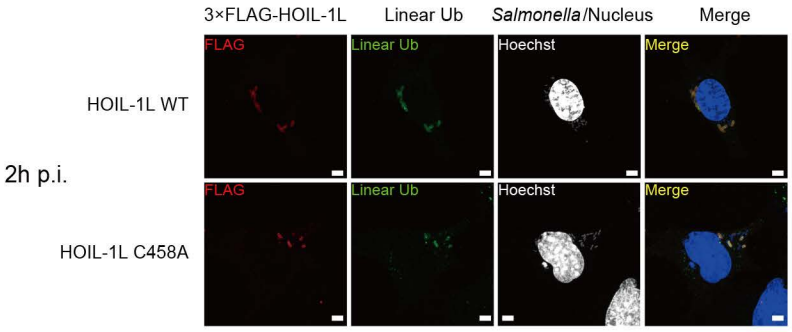

c

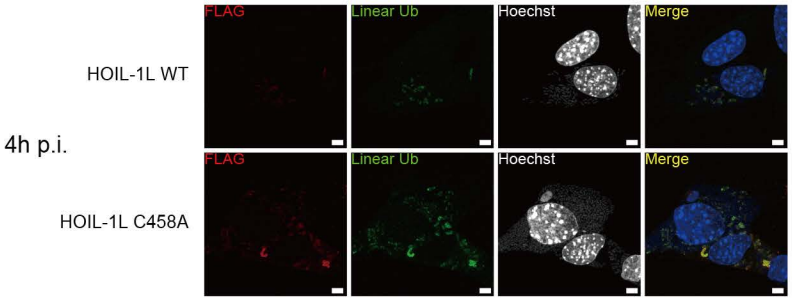

d

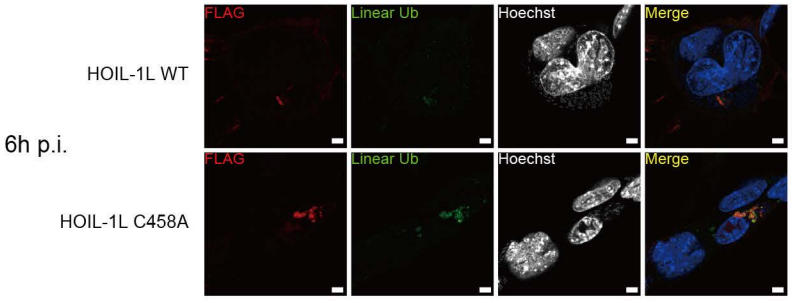

LUBAC TKO MEF reconstituted with HOIP and SHARPIN

Fuseya et al. Extended Data Figure6

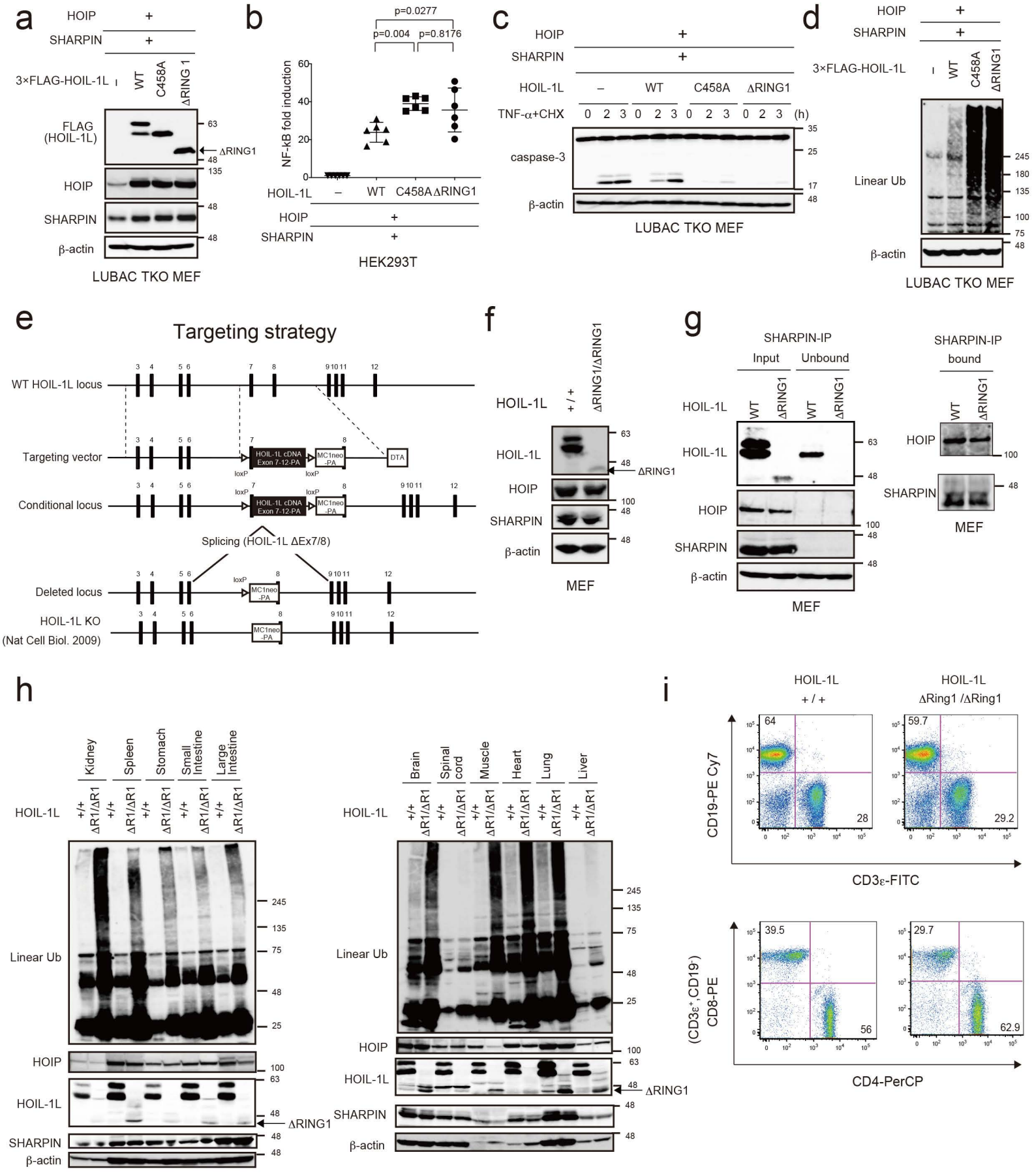

Fuseya et al. Extended Data Figure7

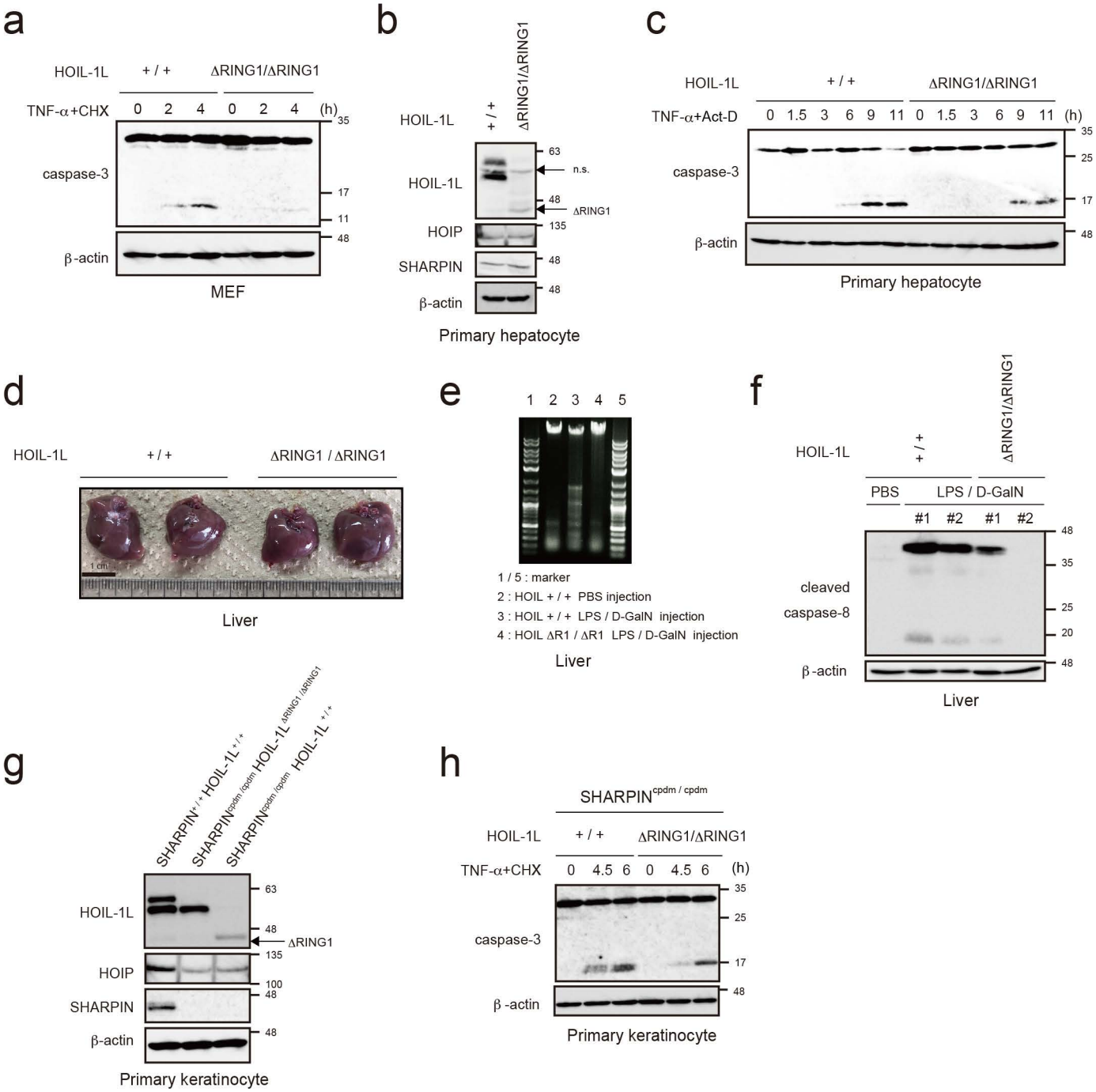

Fuseya et al. Extended Data Figure8

Extended Data Fig. 1 | The highly conserved HOIL-1L RBR ubiquitin ligase negatively regulates LUBAC functions.

a, Conserved residues in the RING1-IBR-RING2 domains of HOIL-1L in the indicated species. Arrow indicates the catalytic cysteine of HOIL-1L. **b**, Schematic representation of mouse HOIL-1L and its mutants. Cleavage of caspase-3 in LUBAC TKO MEFs stably reconstituted with HOIP and the indicated HOIL-1L protein, stimulated with TNF-α (3 ng ml^{-1}) and CHX (20 μg ml^{-1}), was assessed by immunoblotting. The experiments were repeated twice, independently, with similar results. **c**, Viability of LUBAC TKO MEFs stably reconstituted with HOIP, SHARPIN, and the indicated HOIL-1L protein, stimulated with TNF-α (10 ng ml^{-1}), was measured using the iCELLigence system. The experiments were repeated three times, independently, with similar results. **d**, NF-κB activation in HEK293T cells transfected with the indicated expression plasmids and 5× NF-κB luciferase reporters was measured by luciferase assay. Mean is shown; n=3 independent experiments; *P*-values are from a two-tailed Student's t-test. **e**, Quantitative PCR (qPCR) analyses of expression levels of NF-κB target genes in LUBAC TKO MEFs stably reconstituted with HOIP, SHARPIN, and the indicated HOIL-1L protein. Mean ± S.D. is shown; n=5 independent experiments; *P*-values are from a two-tailed Student's t-test. **f,** Phosphorylation and degradation of IκBα in LUBAC TKO MEFs stably reconstituted with HOIP and SHARPIN. The experiments were repeated three times, independently, with similar results. Data and unprocessed blots are available as source data.

Extended Data Fig. 2 | Loss of HOIL-1L E3 does not overtly affect K48, K63, or other types of chains.

a, Amounts of the indicated types of ubiquitin chains in LUBAC TKO MEFs stably reconstituted with HOIP and SHARPIN, and the indicated HOIL-1L protein. Lysates from TKO MEFs expressing the indicated HOIL-1L proteins were probed with the indicated antibodies. The experiments were repeated three times, independently, with similar results. **b**, Assessment of ubiquitin linkages in lysates of LUBAC TKO MEFs stably reconstituted with HOIP, SHARPIN, and the indicated HOIL-1L protein using MS analyses. Mean is shown; n=3 independent experiments; *P*-values were obtained by one-way ANOVA followed by Tukey's multiple comparison test. Data and unprocessed blots are available as source data.

Extended Data Fig. 3 | Auto-ubiquitination of HOIL-1L inhibits LUBAC functions.

a, Lysates of LUBAC TKO MEFs stably reconstituted with HOIP C879A, SHARPIN, and the indicated HOIL-1L protein were probed as depicted. Arrow shows the upper band of HOIL-1L. **b**, *In vitro* ubiquitination reactions were performed at 37℃ for 24 h with His-UBCH7 C/S to generate an oxy-ester bond between ubiquitin and UBCH7, followed by digestion of ubiquitinated UBCH7 with NH_2OH or USP2cc at 37°C for 1 h. **c,h,l** Lysates of indicated MEFs were probed as depicted. **d**,**i** Digestion of the upper (modified) HOIL-1L signal with USP2cc or NH_2OH at 37°C for 30 min anti-FLAG immunoprecipitates obtained under denaturing conditions from LUBAC TKO MEFs expressing 3×FLAG–HOIL-1L WT (**d**) or the All-K/R mutant (**i**). **e,j,k**, LUBAC TKO

MEFs stably reconstituted with HOIP, SHARPIN and 3×FLAG-HOIL WT (**e**) or the All-K/R mutant (**j,k**) were subjected to mass spectrometry to assess ubiquitination sites in LUBAC subunits. S107 of hHOIP (e), S915 of mHOIP (j), and T955 of mHOIP (k) were identified as ubiquitination sites. **f**, Lysates of HEK293T cells transfected with the indicated expression plasmids were probed as indicated. **g**, NF-κB activation in HEK293T cells transfected with the indicated expression plasmids and 5×NF-κB luciferase reporters was assessed by luciferase assay. Mean is shown; n=3 independent experiments; *P*-values are from a two-tailed Student's t-test.

The data shown were repeated twice, independently, with similar results. Data and unprocessed blots are available as source data.

Extended Data Fig. 4 | Loss of HOIL-1L E3 activity increases LUBAC activity *in vitro*.

a, b, Linear ubiquitin (**a**) or modification of indicated HOIL-1L proteins (**b**) in *in vitro* ubiquitination assays with Petit-SHARPIN and HOIL-1L WT or the indicated mutants, as assessed by immunoblotting. The data shown were repeated three times, independently, with similar results. Unprocessed blots are available as source data.

Extended Data Fig.5 | HOIL-1L ubiquitinates all LUBAC subunits, HOIP conjugates linear ubiquitin onto the ubiquitin, and OTULIN counteracts this effect.

a, Modification of LUBAC subunits in WT or OTULIN KO MEFs treated or not treated with lysates containing MBP-OTULIN at 37°C for 1 h. * shows non-specific bands. The

experiments were repeated three times, independently, with similar results. **b**, Schematic representation of HOIL-1L WT and ΔRING1 (lacking aa 251–341). **c**, Cleavage of caspase-8 and caspase-3 induced by TNF-α (1 ng ml^{-1}) plus CHX (20 μg ml^{-1}) in WT or OTULIN KO MEFs expressing the indicated HOIL-1L proteins. The experiments were repeated twice, independently, with similar results.

Unprocessed blots are available as source data.

Extended Data Fig. 6 | Loss of HOIL-1L E3 protects against *Salmonella typhimurium* infection, and infecting *S. typhimurium* are covered with high levels of linear ubiquitin in MEFs expressing ligase-defective HOIL-1L.

a-d, *S. typhimurium* infections of LUBAC TKO MEFS stably expressing HOIP, SHARPIN, and 3×FLAG–HOIL-1L WT or C458A. Microscopic images of indicated MEFs were collected 24 hours after infection. Scale bars, 500 μm **(a)**. Confocal micrographs of LUBAC TKO MEFs stably expressing HOIP, SHARPIN, and 3×FLAG–HOIL-1L WT or C458A were infected with *S. typhimurium* and stained for linear ubiquitin (1E3), FLAG (M2), or Hoechst 33342 at 2 h (**b**), 4 h (**c**), and 6 h (**d**) post-infection. Scale bars, 5 μm **(b–d)**.

The data shown were repeated three times, independently, with similar results.

Extended Data Fig. 7 | Generation of HOIL-1L ΔRING1 mice as a model for ligase-defective HOIL-1L mice.

a, LUBAC TKO MEFs stably reconstituted with the indicated proteins were probed as shown. **b**, NF-κB activation in HEK293T cells transfected with the indicated expression plasmids and 5× NF-κB luciferase reporters was assessed by luciferase assay. Mean ± S.D. is shown; n=6 independent experiments; *P*-values are from one-way ANOVA followed by Tukey's multiple comparison test. **c**, Cleavage caspase-3 in LUBAC TKO MEFs stably reconstituted with the indicated proteins and stimulated with TNF-α (2.5 ng ml^{-1}) plus CHX (20 μg ml^{-1}) was assessed by immunoblotting. **d**, Level of linear ubiquitin in LUBAC TKO MEFs stably reconstituted with the indicated proteins. **e**, Schematic representation of conditional and deleted loci of HOIL-1L conditional ΔRING1 mice. **f,** Cell lysates of primary MEFs from WT and HOIL-1L ΔRING1 mice were probed as indicated. **g,** Indicated MEFs were immunoprecipitated with anti-SHARPIN antibody, and bound and unbound fractions were probed as indicated. **h,** Lysates of the indicated organs from 8-week-old littermate mice of the indicated genotypes were probed as depicted. **i,** Splenocytes of 15-week-old littermate mice of the indicated genotypes were examined by flow cytometry. Splenocytes were analyzed for surface expression of CD3 and CD19 (upper panels) and T cell subpopulations of splenocytes were analyzed for surface expression of CD4 and CD8 (lower panels). Experiments were repeated independently with similar results twice (a,c,g,h,i) or at least three times (d,f). Data and unprocessed blots are available as source data.

Extended Data Fig. 8 | Pathophysiological roles of HOIL-1L ΔRING1 in mice.

a, Primary MEFs from WT and HOIL-1L ΔRING1 mice were probed as depicted after

stimulation with TNF-α (5 ng ml-1) plus CHX (20 μg ml-1) for the indicated periods. **b**, Lysates of primary hepatocytes from 12-week-old WT or HOIL-1L ΔRING1 mice were probed as indicated. **c**, Cleavage of caspase-3 in primary hepatocytes from 12-week-old WT or HOIL-1L ΔRING1 mice after stimulation with TNF-α (10 ng ml-1) plus actinomycin D (Act-D) (100 ng ml-1) was assessed by immunoblotting. **d**, Macroscopic appearance of livers of the indicated mice at 18 weeks old. Scale bar, 1 cm. **e,f,** Mice of the indicated genotypes were injected intraperitoneally with LPS/D-GalN or PBS. Seven hours after injection, DNA ladder (**e**) or cleaved caspase-8 (**f**) in liver lysates of the indicated mice was probed as depicted. **g,** Primary keratinocytes from 7-week-old WT or HOIL-1L ΔRING1 mice were probed as indicated. **h**, Cleavage of caspase-3 in primary keratinocytes from 7-week-old WT or HOIL-1L ΔRING1 mice after stimulation with TNF-α (10 ng ml-1) plus CHX (20 μg ml-1) was assessed by immunoblotting.

Experiments were repeated independently with similar results twice (a,c,e-h) or at least three times (b,d). Unprocessed blots are available as source data.

Supplementary Figure1: Gating strategy for flow cytometry analysis

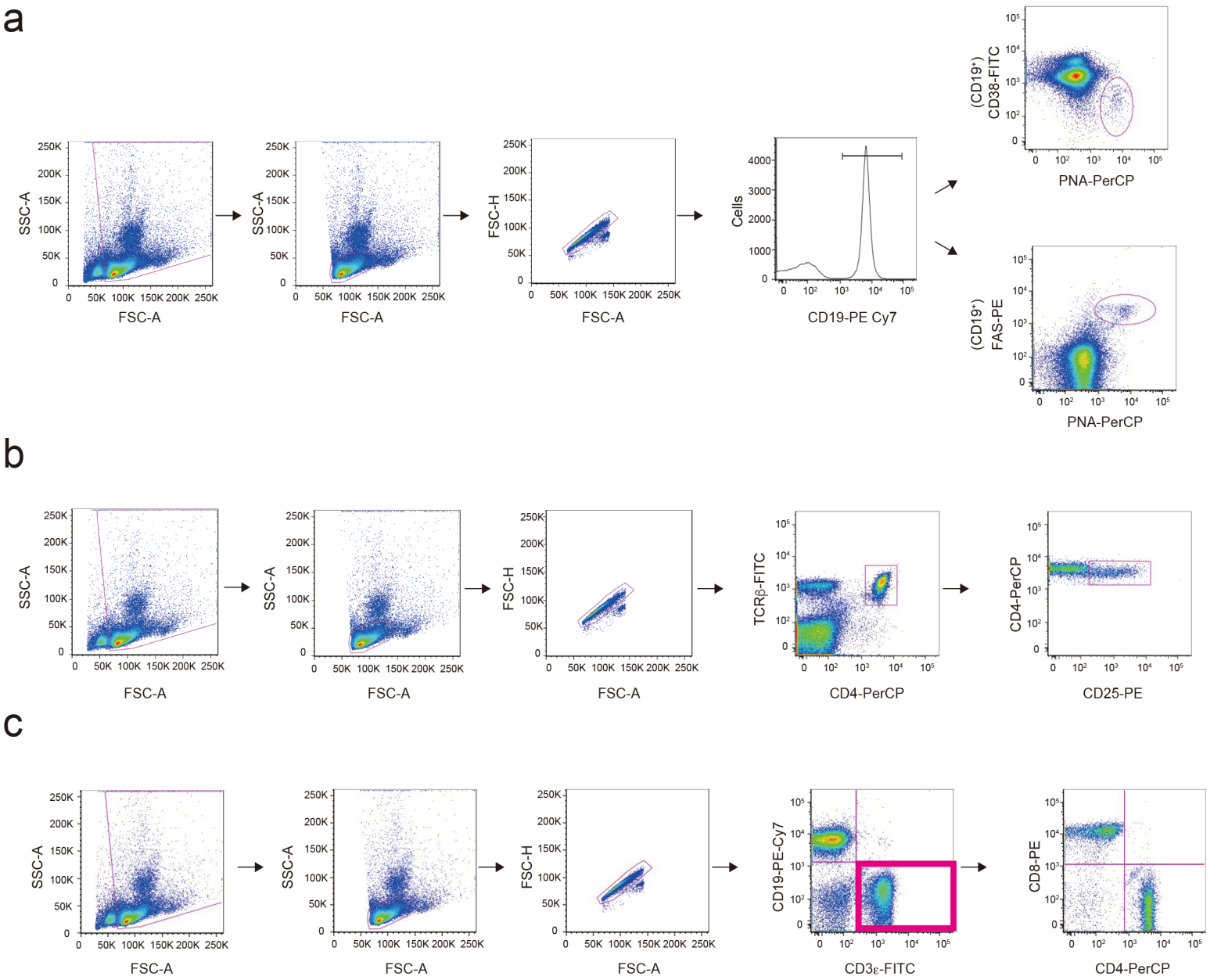

a-c, Single-cell suspensions prepared from the spleen of 8- to 15-week-old mice of the indicated genotype were stained with fluorochrome-conjugated antibodies. Live lymphocytes were gated with forward-scatter (FSC) and side-scatter (SSC), and FSC-area (FSC-A) and FSC-height (FSC-H) were used to discriminate single cells from doublet and multiplet cells. $CD19^+$ B cells of splenocytes were analyzed for surface expression of CD38 and PNA, or FAS and PNA (a). $TCR\beta^+CD4^+$ T cells of splenocytes were analyzed for surface expression of CD25 (b). Splenocytes were analyzed for surface expression of CD3ε and CD19, and $CD19^-CD3\varepsilon^+$ cells were analyzed for surface expression of CD4 and CD8 (c).